Precise sediment flux assessment of a small ungauged low-mountain catchment in the North Caucasus

Anatoly Tsyplenkov (atsyplenkov@gmail.com)
Institute of Geography Russian Academy of Science https://orcid.org/0000-0003-4144-8402
Sergey Kharchenko
Institute of Geography Russian Academy of Science
Maxim Uspensky
Lomonosov Moscow State University
Simon Scheper
Dr. Simon Scheper - Research | Consulting | Teaching https://orcid.org/0000-0001-8097-673X
Valentin Golosov
Institute of Geography Russian Academy of Science https://orcid.org/0000-0002-4351-8323

Research Article

Keywords: sediment yield, soil erosion, RUSLE, North Caucasus, sedimentation rate, erosion mapping, denudation

Posted Date: October 18th, 2022

DOI: https://doi.org/10.21203/rs.3.rs-2179933/v1

ABSTRACT

Soil erosion and sediment export from hillslopes are significant problems associated with agriculture, especially in parts of the world where society is already living in extreme environments. In particular, mountainous environments remain severely understudied, with only a few runoff and sediment transport measurements available. It is necessary, therefore, to develop and validate independent methods that do not rely on long-term observations at gauging stations.

Here we used three independent methods to predict soil erosion and associated sediment yield (SY) from a 1.84 km² basin in the North Caucasus. The first part concerns assessing the sedimentation rate, which was made using in-situ measurements of volumetric sediment deposition rates. Secondly, we look at the connectivity of sediment sources and the lake. A combination of remote sensing data and field surveys was used to estimate sediment connectivity and erosion mapping. The third part regards the computation of soil erosion using the Revised Universal Soil Loss Equation (RUSLE).

There are three major findings in this study that help us understand sediment redistribution patterns in mountainous areas. First, based on the lake sedimentation rate, we found that the mean annual area-specific sediment yield is 514 (95% CI, 249–839) t km^{-2} yr^{-1}. Similar results were obtained from the erosion mapping (i.e., a map of erosion processes) — 428 (95% CI, 322–546) t km^{-2} yr^{-1}. Secondly, the spatial distribution and rates of the erosion processes suggest that sheet and rill erosion are responsible for *ca.* 40% of total sediment export, slides and rockfalls — 18%, while the rest is removed by soil creep. Additionally, the RUSLE-based modelling of sheet wash and rill erosion has highlighted the areas most prone to soil erosion. The corresponding mean annual soil erosion rate of 1.59 mm yr^{-1} was very close to the results obtained from the literature review.

1. INTRODUCTION

To meet the rising demand for food without compromising the ecosystem's health, there is an urgent need for sustainable intensification of agriculture to meet Sustainable Development Goal 2. However, soil erosion and sediment export from hillslopes are significant problems associated with agriculture, especially in parts of the world where society is already living in extreme environments, especially mountain regions such as the Caucasus (Forte et al., 2016; Golosov and Tsyplenkov, 2021; Perov et al., 2017; Vezzoli et al., 2020). At a river basin scale, soil erosion threatens food, water, and energy security due to the loss of productive soil and nutrients from hillslopes, pollution of downstream water bodies by sediment and contaminants (Ivanov et al., 2021), and siltation of hydropower dams and reservoirs (Hasholt et al., 2000; Syvitski et al., 2022). The challenges of sediment dynamics are becoming increasingly pressing with population growth, agricultural expansion, and climate change (Dethier et al., 2022).

Furthermore, different processes of denudation contribute to river sediment yield (SY). Many studies (Blake et al., 2018; Carrillo and Mao, 2020;

Navas et al., 2020; Tsyplenkov et al., 2021a) aim to understand better the role and relative importance of different sediment sources (e.g., landslides, riverbank erosion, glacial erosion) in such environments. Akin insights are highly needed for understanding erosion and sediment transport at various spatial scales, notably in the face of climate and land-use changes.

This problem is particularly relevant to ungauged regions, which account for most of the Earth's surface (Hrachowitz et al., 2013), where it is challenging to estimate SY and water runoff (Pool et al., 2017). In particular, mountainous environments remain severely understudied, with only a few runoff and sediment transport measurements available (Vanmaercke et al., 2011). The low mountain topographic zone (500–1500 m) of the North Caucasus is not an exception (Golosov and Tsyplenkov, 2021). Historically, pastoralism and animal husbandry have been important forms of agriculture in the region (Holland, 2016; Hovsepyan, 2015). However, the collapse of the Soviet Union reduced population density in the mountains (Vinogradova et al., 2018), causing summer pastures to be abandoned and stationary grazing to occur (Lewińska et al., 2021). Such significant changes in land use patterns, combined with climate warming (Toropov et al., 2019), have resulted in the expected altering of SY (Tsyplenkov et al., 2021b) over the last decades.

No matter the fact that the population density there is among the highest in the Great Caucasus region (Vinogradova et al., 2018), the gauging station density is low (Rets et al., 2020), especially the ones measuring sediment transport (Golosov and Tsyplenkov, 2021). The results from gauging measurements alone may not always indicate the regional SY patterns (Vanmaercke et al., 2012, 2014). It is necessary, therefore, to develop and validate independent methods that do not rely on long-term observations at gauging stations. One way to offer an SY estimate accessible for a relatively short period (Hadley et al., 1984) is by measuring a reservoir sedimentation rate (Verstraeten and Poesen, 2002). The sediment deposition rate may nevertheless provide the extent of catchment erosion; however, reservoir characteristics substantially impact the sedimentation values (Verstraeten and Poesen, 2000). Moreover, a significant SY uncertainty may occur if the volumetric sedimentation rate is not accurately determined (Reinwarth et al., 2019).

A variety of models exist for SY prediction at a regional scale, but not all are critically evaluated or represent only selected processes (de Vente et al., 2013). The Revised Universal Soil Loss Equation (RUSLE, Renard et al. (1997)) is currently the most widely used erosion model in the world (Borrelli et al., 2021), but estimates only sheet and rill erosion. However, its adaptation to mountainous areas can cause several issues, relating mainly to the quantitative description of hillslopes (Bircher et al., 2019). Using RUSLE alone can lead to a misunderstanding of sediment transport processes (Govers, 2010), and independent assessment is crucial for model evaluation (Batista et al., 2021). Thus, for the mountain catchments, the best results can be obtained by combining several approaches, including field surveying, erosion modelling, and remote sensing to evaluate sediment redistribution (Heckmann et al., 2016; Heckmann and Schwanghart, 2013; Messenzehl et al., 2014). Generally, sediment yield isn't measurable directly but can be estimated with sediment delivery ratio (SDR) — a percentage of gross basin erosion delivered

to the river network (Walling, 1983). However, an SDR estimation cannot be done precisely, and various approaches exist (Najafi et al., 2021). For example, modelling sediment connectivity based on detailed digital elevation models (DEM) and other remote sensing data can help quantify certain aspects of sediment transfers (Cavalli et al., 2013).

In this context, we performed a retrospective sediment budget analysis of the small mountain lake in the North Caucasus — Gizhgit-Syr lake near Tyrnyauz (Kabardino-Balkarian Republic). This catchment was chosen because we hypothesised that sediment transport there is generated solely by slope processes. It also meets the requirements for lakes to be used to reconstruct the denudation rate (Mills et al., 2017; Schillereff et al., 2014), i.e. small catchment size (A = 1.84 km^2), simple shoreline morphometry and a maximum depth of 4 m. We aim to estimate the relative role of various hillslope transport processes using three independent methods: measuring lake siltation rate, soil erosion modelling and geomorphological mapping with sediment connectivity modelling. Our findings may help inform how sediment transport forms in a typical catchment for the low mountain topographic zone of the North Caucasus with long-term free grazing practices.

2. STUDY AREA

The Gizhgit-Syr catchment is located on the left valley bank of the Baksan River, the left tributary of the Terek River (see Figure 1). The waterbody at the catchment outlet can be classified as a pond (Richardson et al., 2022). It will, however, be referred to hereinafter as the Gizhgit-Syr lake since that is how it has historically been described on maps.

2.1 Geomorphological and geographical settings

The Gizhgit-Syr catchment lies on the periphery of the Scalisty (Rocky) Range of the Greater Caucasus, characterised by typical for the region cuesta-like morphology. Cuestas originate due to the monoclinal occurrence of the Middle Jurassic terrigenous-organogenic sedimentary complexes (Dzhora and Gandalbos formations) with the dip direction from the axial zone of the Greater Caucasus to its northern periphery. In the lower part of the section, they are represented by argillites, siltstones, and sandstones, and in the upper part, by limestones, gypsum, dolomites, and carbonate mudstones (Andrushhuk et al., 1968).

The Gizhgit-Syr catchment is a left-bank tributary of the Gizhgit River (cf. Figure 1). The left side of the parent Gizhgit River basin is a steeper escarpment of scarp slope, prone to erosion. The right side of the valley is a dip slope, gentler, almost without outcrops of bedrock, with a predominance of soil mass displacement processes. The small Gizhgit-Syr catchment is located entirely on a steeper valley slope, resulting in precipitous slopes, bedrock protrusions, and low loose sedimentary cover of 5-40 cm (See Figure S0).

Mean Gizhgit-Syr catchment elevation is 1427 m a.m.s.l., the outlet is located at 1176 m a.m.s.l. Therefore, the studied area could be considered a Low Mountain catchment, according to the LANMAP2 classification (Mücher et

al., 2006). The Gizhgit-Syr is characterised by a temperate mountainous climate with a mean annual rainfall of about 700 mm (Funk et al., 2015).

The slopes are variously sodded, which can be explained by the use of the catchment for livestock grazing, which was more intensive in the recent past. This is evidenced by the remaining remnants of cattle sheds (see Figure S0). Tree and shrub vegetation is presented mainly along the bottom of the main valley.

2.2 Gizhgit-Syr lake history

The Gizhgit-Syr lake was previously part of the larger tailing pond (Ullu-Gizhgit lake) created for the needs of the Tyrnyauz Tungsten-Molybdenum Mining and Processing Complex (TTMC) on the Gizhgit River, a left tributary of the Baksan River. The TTMC was constructed started 1939 and commissioned in 1945 (Bortnikov et al., 2020), mining the largest Tungsten skarn deposit in the Former Soviet Union (Soloviev et al., 2021). According to aerial photos and historical maps, the dam was tentatively built in 1964-1965 (see Figure S1). Nevertheless, the inundation of the Gizhgit-Syr valley began only in 1989, and until 2000 the Gizhgit-Syr and Ullu-Gizhgit were connected (see Figure S1). The Ullu-Gizhgit was a tailing impoundment until 2003, when the TTMC was decommissioned (Bortnikov et al., 2020). Therefore, it was filled by a mixture of water and tailings gradually upstream from the dam. As a result, some tailings may have been transferred into the studied waterbody during the 1989–2000 period, but this aspect has not yet been examined. There is no doubt that the Gizhgit-Syr lake has been endorheic since 2000 (see Figure S1), having a 100% trap efficiency.

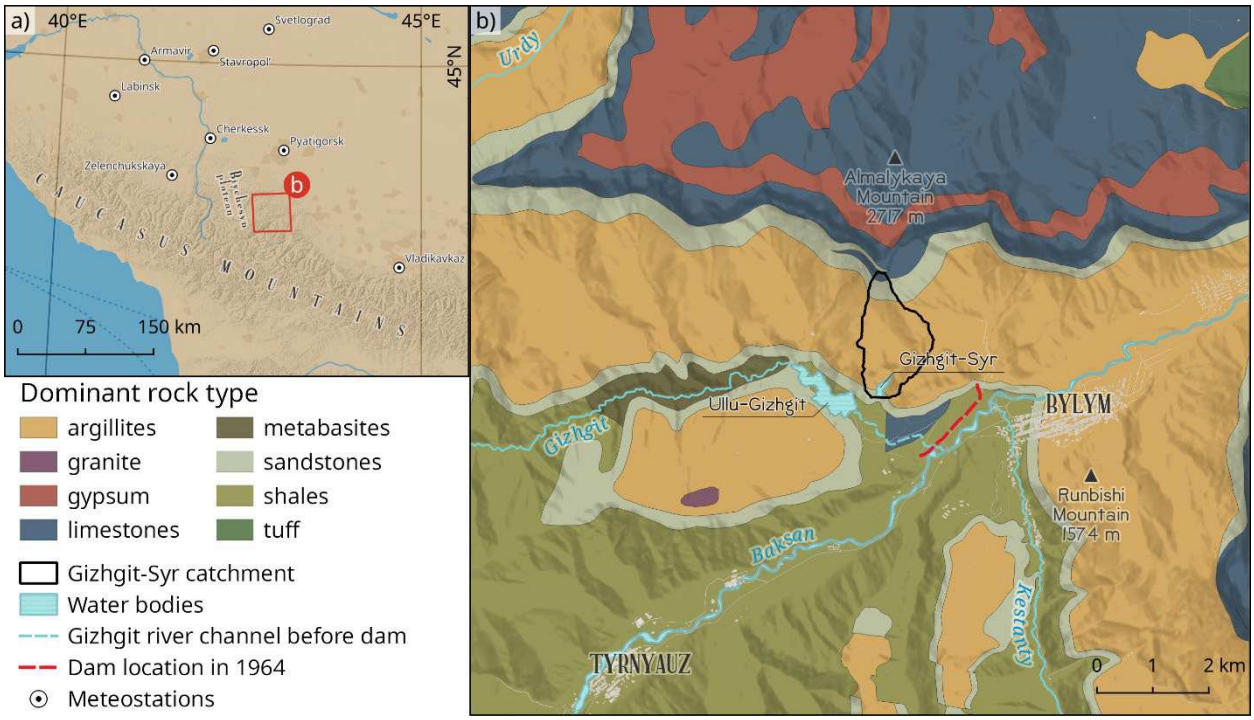

FIGURE 1. Map (a) shows the study area's location in the Caucasus region. Fragment of Geological map (Pismenny et al., 2021) on the study area showing the interpreted dominant rock type (b).

3. MATERIALS AND METHODS

The methodology can be divided into three parts. The first part concerns assessing the sedimentation rate, which was made using *in-situ* measurements of volumetric sediment deposition rates. Secondly, we look at the connectivity of sediment sources and the lake. A combination of remote sensing data and field surveys was used to estimate sediment connectivity and erosion mapping. The third part regards the computation of soil erosion using the Revised Universal Soil Loss Equation (RUSLE). These methods are summarised below, and where applicable, additional detail is included in a Supplement.

3.1 Remote sensing data

A high-resolution elevation dataset was acquired with Unmanned Aerial Vehicles (UAVs) and photogrammetric processing. Additionally, accurate measurements of DGPS reference points were used to obtain an independent source of ground elevation data. In August 2020 and May 2021, aerial surveys were conducted with a DJI Mavic Pro. Nadir images were taken from a height of 100-300 meters overlapping on the front and sides. Oblique images were sparsely captured so that hidden areas could be better covered. For calibration purposes of the photogrammetric evaluation, the South S660N DGPS device was used to measure ground control points. The drone imagery was further processed using the Structure-from-Motion (SfM) photogrammetry software Agisoft Photoscan, resulting in a digital terrain model (DTM) resolution of 0.27 cm/pix, which was harmonised to 1 m cell size. It was further filtered using SAGA's simple square filter with a 5m radius and filled with Wang and Liu's (2006) algorithm. The overall quality of the resulting DTM is 0.06 ± 0.4 m (see Figure S2 for details).

3.2 Lake bathymetry data

The lake bathymetry was carried out during a field campaign in August 2020 using a Deeper Chirp+ echo sounder. This device is a single-beam sonar with a 675 kHz frequency (7° beam angle). With such settings, the sonar has a minimum measuring depth of 0.15 m and an anticipated vertical error of 0.11 m (Bandini et al., 2018). A further bathymetry map was created in Reefmaster 2.0.38 (see Figure 2a). This software uses TIN interpolation with Gaussian smoothing by default. The resulting DEM was compared with sonar measurements (see Figure S3 for details). We found the vertical accuracy of interpolation to be −0.03 ± 0.28 m.

3.3 Sediment deposition rate

Using a gouge auger (⌀ 2 cm), thickness surveys were conducted to map the thickness of the bottom deposits (see Figure 2b) in August 2020. A total of 21 measurements were taken, evenly spatially distributed across the lake. To interpolate sediment thickness over the entire lake area (to a 1×1 m grid), we fitted a generalised additive model (Thin Plate Regression Spline (Wood et al., 2008)) to predict thickness with coordinates (X, Y) and depth. Model parameters were estimated using restricted maximum likelihood (REML) and

outer optimiser using the mgcv R package (Wood, 2011). The model exploratory power is substantial (R^2 = 0.83) with RMSE equal to 0.098.

As a result of the sediment thickness map (Figure 2b), the volume of lake deposits (V, m^3) was calculated as the sum of all grid cells. This value was further used to assess the sediment yield following the Verstraeten and Poesen approach (2002):

$$SY_{Lake} = \frac{dBD \cdot V}{T_L \cdot A}, \quad (1)$$

where SY is the area-specific sediment yield (t km^{-2} yr^{-1}); dBD is the dry bulk density of the lake deposits (t m^{-3}); T_L is the period in years during which the sediments were accumulated; A is the catchment area (km^2).

Using satellite images (see Figure S1), we can infer that the valley has been flooded since 1989, while the survey was conducted in 2020. Since the two waterbodies were hydraulically connected, tailings and sediments might be transported from Ullu-Gichgit to Gizhgit-Syr after 1989 till 2000. Moreover, even after 2000, some evidence (see rills in Figure S1) indicates that sediments from the drained dam may enter the Gizhgit-Syr outside the basin. Consequently, additional sediment input may have skewed the measured basin sediment export. Because we are unable to separate basin sediments from tailings at this stage, we have chosen to examine two periods of sediment deposition: 1989–2020 (T_L = 31 yr) and 2001–2020 (T_L = 20 yr).

We know that the approach is rough and involves several shortcomings and errors. First, as hammer-driven augers are driven into the ground, they may compact the sediment, resulting in possible errors in sediment thickness measurements (Garrison, 2016). Additionally, we did not determine bulk density during sediment thickness measurements. The bulk density of sediment differs depending on the sediment texture; therefore, frequent and intensive sampling is necessary to obtain a representative result (Verstraeten and Poesen, 2001b). Moreover, a 2001st study suggests that bulk density variability for submerged and less consolidated sediments within a sediment layer can be up to 60% (Verstraeten and Poesen, 2001a).

To assess the dry bulk sediment density for the Gizhgit-Syr lake, we sampled 1000 values from a truncated normal distribution. The parameters for the distribution were taken from the literature for nearby lakes. Thus, the minimum possible density was set to 0.75 t m^{-3} as for the Khuko lake (Ivanov et al., 2022), while the maximum to 2 t m^{-3} as for the Donguz-Orun lake (Alexandrin et al., 2018). The mean and standard deviation was set to 1.5 and 0.5, respectively, following the distributions from Verstraeten and Poesen's (2001a) study.

In light of a limited number of sediment thickness measurements and the primitive nature of the assessment, the results should be interpreted with caution. However, we assume that the actual sediment yield belongs to our distribution.

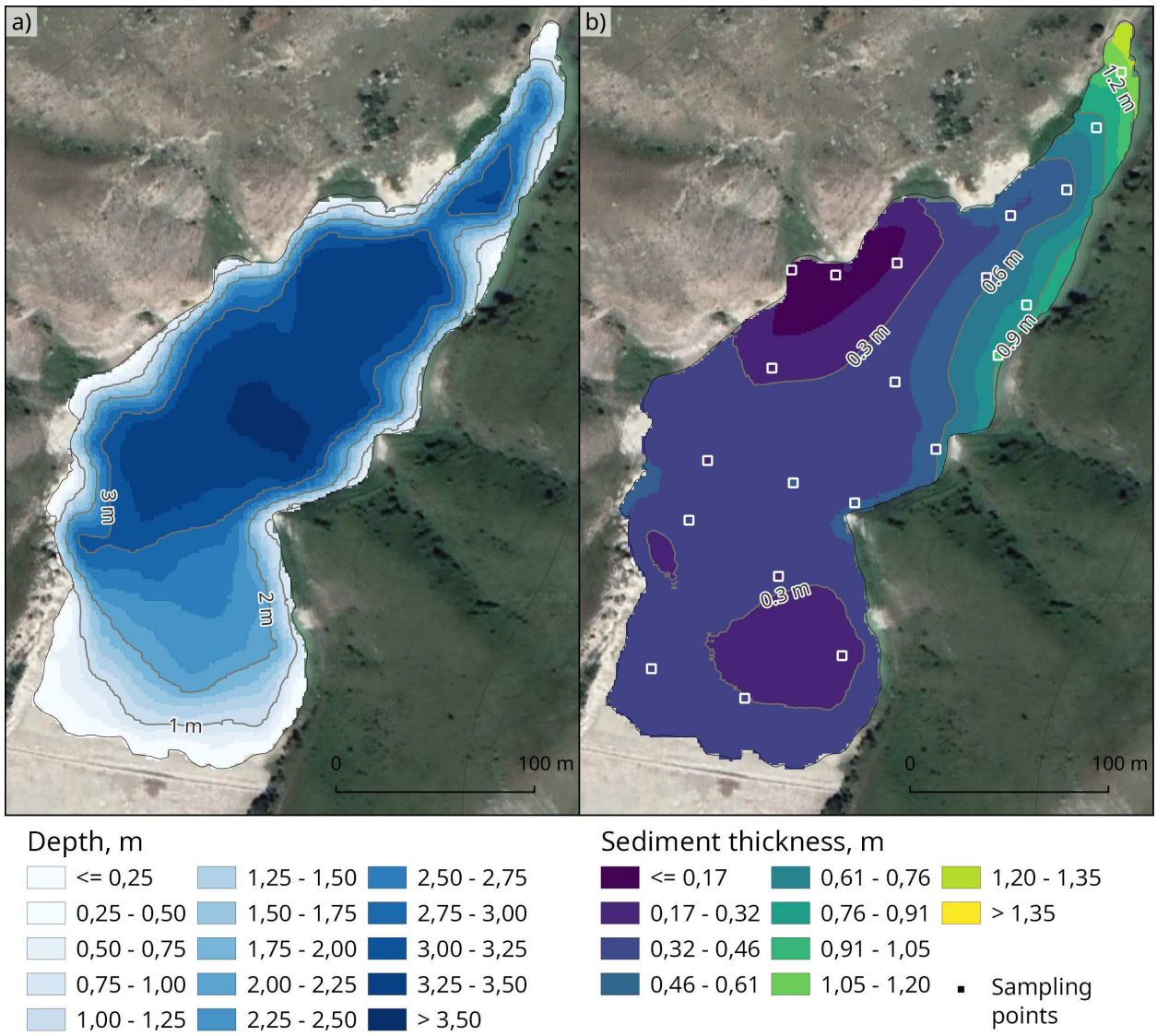

FIGURE 2. Lake bathymetry (a) and sediment thickness (b) map

3.4 Sediment connectivity

In this study, we used a topography-based sediment connectivity index — index of connectivity (IC). This dimensionless index was suggested by Borselli et al. (2008) and adapted for mountain environments by Cavalli et al. (2013). We calculated IC using the standalone executable SedInConnect 2.3 (Crema and Cavalli, 2018), which employs the original Borselli's equation and roughness index (RI) as a weighting factor ($\bar{W}$):

$$IC_i = \log_{10}\left(\frac{D_{up}}{D_{dn}}\right) = \log_{10}\left(\frac{\bar{W}\bar{S}\sqrt{A}}{\sum_i \frac{d_i}{S_i W_i}}\right), \quad (2)$$

where D_{up} is the upslope component; $\bar{W}$ and $\bar{S}$ are the average value of the weighting factor and the average slope (m/m) of the upslope area, respectively, and A is the contributing area (m^2) of pixel i. D_{dn} is the downslope component; d_i is the length (m) of the path along the ith cell, W_i is the weighting factor, and S_i is the slope gradient along the ith cell. The weighting factor was calculated using the roughness index RI — standard deviation of the residual topography on a scale of a few meters (Cavalli et al., 2008; Cavalli and Marchi, 2008).

Erosion by water and fluvial sediment delivery are related by sediment delivery ratio (SDR). The SDR was calculated following the formula suggested by Vigiak et al. (2012) for every *i* cell. Since it was based on IC calculated using Cavalli et al. (2013) approach, from now on denoted as $SDR_{Cavalli}$:

$$SDR_{Cavalli,\ i} = \frac{SDR_{max}}{1+\exp\left(\frac{IC_0 - IC_i}{k}\right)}, \quad (3)$$

where IC_i is the connectivity index for pixel *i*; IC_0 and *k* are calibration parameters defining the *IC–SDR* relationship shape. They were set to 0.5 and 1 accordingly, following Vigiak et al. (2012). SDR_{max} is a theoretical maximum of *SDR* defined as fraction of topsoil particles finer than coarse sand. The SDR_{max} value for the Gizhgit-Syr catchment was derived from the SoilGrids database (Hengl et al., 2017) and set to 0.87. It was based on the CFVO map (volumetric fraction of coarse fragments), which ranged from 0 to 0.6, with an average of 0.13 for the catchment area.

To compare topography-based $SDR_{Cavalli}$ with measured sediment deposition and estimated erosion rates, an independent SDR assessment was conducted. In its original definition, SDR referred to the ratio of sediment export (SE) to gross sediment loss (SL) in a catchment (Walling, 1983). Therefore, we calculated SDR_{Manual} as follows:

$$SDR_{Manual} = \frac{SE}{SL}, \quad (4)$$

where *SE* is a sediment export in t yr^{-1} calculated from the sediment deposition rate (see Section 3.3); *SL* is a total sediment loss (t yr^{-1}) estimated from mean erosion rates (see Section 3.5). Therefore, *SE* can be quantified with Eq. (5), where both $SDR_{Cavalli}$ and SDR_{Manual} are applicable:

$$SE = A_{cell} \cdot Erosion_{rate} = SL \cdot SDR \quad (5)$$

In addition to Eq. (1), area-specific sediment yield (SY, t km^{-2} yr^{-1}) can be calculated from the SE:

$$SY = \frac{SE}{A} \quad (6)$$

3.5 Erosion mapping and sediment sources inventory

It is well documented that transitions between various erosion processes can be vague (Zweifel et al., 2019). To mitigate this issue in erosion mapping, we focused only on major erosion types for a specific area. According to our field surveys and literature review, the main erosion processes in our study area are rill and inter-rill erosion, slides and rockfalls, sheet wash, and soil creep. We also distinguish areas without pronounced erosion processes (i.e., none).

We used the orthophoto image taken in August 2020 with a 1 cm spatial resolution to map the degraded sites. The differentiation between categories was done based on orthophoto visual assessment by an expert, analysis of slope map and relative visible atmospherically resistant index ($VARI_{rel}$). The original $VARI$ is an atmospherically corrected index for vegetation fraction estimation from RGB bands (Gitelson et al., 2002), calculated as follows:

$$VARI = \frac{R_{green} - R_{red}}{R_{green} + R_{red} - R_{blue}} \quad (7)$$

For our purposes, we rescaled it to a new value range from 0 to 1. Therefore, the greener surface is the higher the $VARI_{rel}$ is (see Table1). Rills are distinguished by among the highest $VARI_{rel}$ values and a distinctly

elongated shape. As well as their relatively compact shape and occurrence on steeper slopes, slides and rockfalls differ from surrounding vegetation by their distinct boundary (Meusburger and Alewell, 2008). It is assumed that sheet wash is dominant at sites with low vegetation cover and vague boundaries (Zweifel et al., 2019). The remaining areas are classified as areas with no prevailing erosion type or low suspectable to erosion. Additionally, we considered the creep to be everywhere, except in areas without pronounced erosion processes (e.g., rock outcrops) and rockfall walls.

Monitoring observations were conducted at two locations to determine the soil erosion and rockfall rate. A 1300 m^2 site with low grass cover was chosen to measure the sheet and rill erosion processes. In the provided area, sheet and rill erosion are evident (see Figure S4). The terrain transformation was assessed by comparing multitemporal DTMs created with UAV surveys conducted at 15-20 m altitude. Except for the altitude, the DTM acquiring process was the same as described in Section 3.1. Two time frames (August 2020–May 2021 and May 2021–July 2021) of DTMs were acquired (see Table S1), suggesting a mean rill incision rate of 1 cm yr^{-1}.

Rockfall rates were estimated based on short-term terrestrial laser scanning (TLS) measurements within c. one year (August 2020 — July 2021). The monitoring station was located on the steep slope of the ravine, where bedrock outcrops were on the surface (see Figure S4). Repeated TLS surveys were conducted from 15-20 m using Leica BLK360 with a 1.5–2 mm instrumental survey error. The resulting DEM of the difference of the rockfall wall had a 2.5 cm resolution (see Figure S7).

Soil creep rates were previously estimated by authors (Azhigirov and Golosov, 1990) at the nearby Biychesyn plateau using the "Young pits" method (Young, 1960). The Biychesyn plateau locates 55 km west (see Figure 1) in the low mountain zone (mean altitude is 1700-1800 m a.m.s.l.). The 1990th study found that mean annual soil creep rates (vertical) varies depending on the slope aspect, steepness, and regolith thickness from 0.94 to 2.86 mm yr^{-1} with 1.92 average mm yr^{-1} (Azhigirov and Golosov, 1990). However, even though the Biychesyn plateau locates nearby, the area's altitude is 300–400 m higher than Gizhgit-Syr's. Therefore, temperature changes pass through 0 °C more frequently during the day. While the freeze-thaw processes, along with moisture fluctuations, are the reason for causing soil creep (Kirkby, 1967), the possible soil creep rates at Gizhgit-Syr's slopes should be lower than 1.92 mm yr^{-1}. We used a value of 1.5 mm yr^{-1} for further calculations as an average for low mountain ranges (Anderson and Cox, 1978; Azhigirov and Golosov, 1990).

TABLE 1 Summary statistics of territories covered by dominant erosion processes and their rates

	Type of erosion process	**Mean (SD) elevation, m**	**Mean (SD) slope, °**	**Mean $VARI_{rel}$**	**Mean erosion rate (m yr^{-1}) used in further calculations**	**Source**
1	Rills incision	1321 (91)	26 (10)	0.81	0.01	This study. See Section

						4.3 for details
2	Slides and rockfalls	1385 (177)	42 (12)	0.06	0.013	This study. See Section 4.3 for details
3	Rill, inter-rill erosion and sheet wash at vegetated slopes	1396 (117)	28 (9)	0	0.0015	(Alewell et al., 2014; Azhigirov, 1991)
4	Soil creep	1473 (202)	28 (9)	1	0.0015	(Anderson and Cox, 1978; Azhigirov and Golosov, 1990)
5	None	1423 (75)	7 (3)	0.88	—	—

Further, the map of erosion processes was used to create a spatially distributed raster of mean annual erosion rates (m yr^{-1}) by reclassifying with the help of Table 1. However, the rockfall rates are estimated on the surface normal while the areas are calculated by projecting the sub-vertical scarps onto the horizontal space. Thus, the actual rockfall volumes may be underestimated. To address this issue, the erosion rates estimated from the normal to the slope were divided by the slope cosine.

To get a sediment loss raster ($SL_{Erosion\,map}$, t yr^{-1}), the erosion rates were multiplied by the bulk density map. The latter was created based on the 1:200 000 scales geologic map in the Soviet geologic map series, specifically K-38-I and K-38-II (see Figure 1b). While map units are determined chronostratigraphically, we transcribed them lithostratigraphically and defined three major rock types in the basin: argillites, sandstones, and limestones (cf. Figure 1b). The dry bulk density (t m^{-3}) was sampled from a truncated normal distribution with mean and standard deviation taken from regional studies (Buachidze et al., 1978). The average bulk density of argillites in the area should be 2.55 t m^{-3}, sandstones — 2.32 t m−3, and limestones — 2.67 t m^{-3}. We hypothesised that the minimum possible bulk density could not be lower than 2.2 t m^{-3}, while the maximum should not exceed 4 t m^{-3} (Buachidze et al., 1978). The standard deviation of 1000 Monte-Carlo runs was set to 1.4. By generating 1000 dry bulk density rasters, all the possible sediment loss values could be obtained.

The resulting sediment export ($SE_{Erosion\,map}$, t km^{-2} yr^{-1}) was estimated by multiplying $SL_{Erosion\,map}$ with $SDR_{Cavalli}$:

$$SE_{Erosion\,map} = SL_{Erosion\,map} \cdot SDR_{Cavalli}, \quad (8)$$

3.6 Soil erosion modelling

Additionally, sheet and rill erosion has been assessed with the detachment-limited model RUSLE (Renard et al., 1997). It estimates the soil loss by multiplying the erosion factors:

$$SL_{RUSLE} = R \cdot K \cdot C \cdot LS \cdot P, \quad (9)$$

where SL_{RUSLE} is mean annual soil loss (t ha^{-1} yr^{-1}), *R* is the rainfall erosivity factor (MJ mm ha^{-1} h^{-1} yr^{-1}), *K* is the soil erodibility factor (t ha h ha^{-1} MJ^{-1} mm^{-1}), *LS* is the slope length and slope steepness factor (dimensionless), *C* is the cover-management factor (dimensionless), and *P* is the support practices factor (dimensionless). An application of the RUSLE model based on the best available datasets for the Gizhgit-Syr basin was performed in this study (see Figure 3). We calculated the mean annual soil loss for the lake's existence period (1989–2020). The resulting RUSLE raster was used to estimate the sediment export from rill and sheet erosion (SE_{RUSLE}, t yr^{-1}) by multiplying the RUSLE soil loss with $SDR_{Cavalli}$:

$$SE_{RUSLE} = SL_{RUSLE} \cdot SDR_{Cavalli}, \quad (10)$$

Similarly, RUSLE-associated area-specific sediment yield (SY_{RUSLE}, t km^{-2} yr^{-1}) was calculated as follows:

$$SY_{RUSLE} = \frac{SE_{RUSLE}}{A}, \quad (11)$$

The overall soil erosion modelling scheme is presented in Figure 3, while the process is described in detail in Supporting Information.

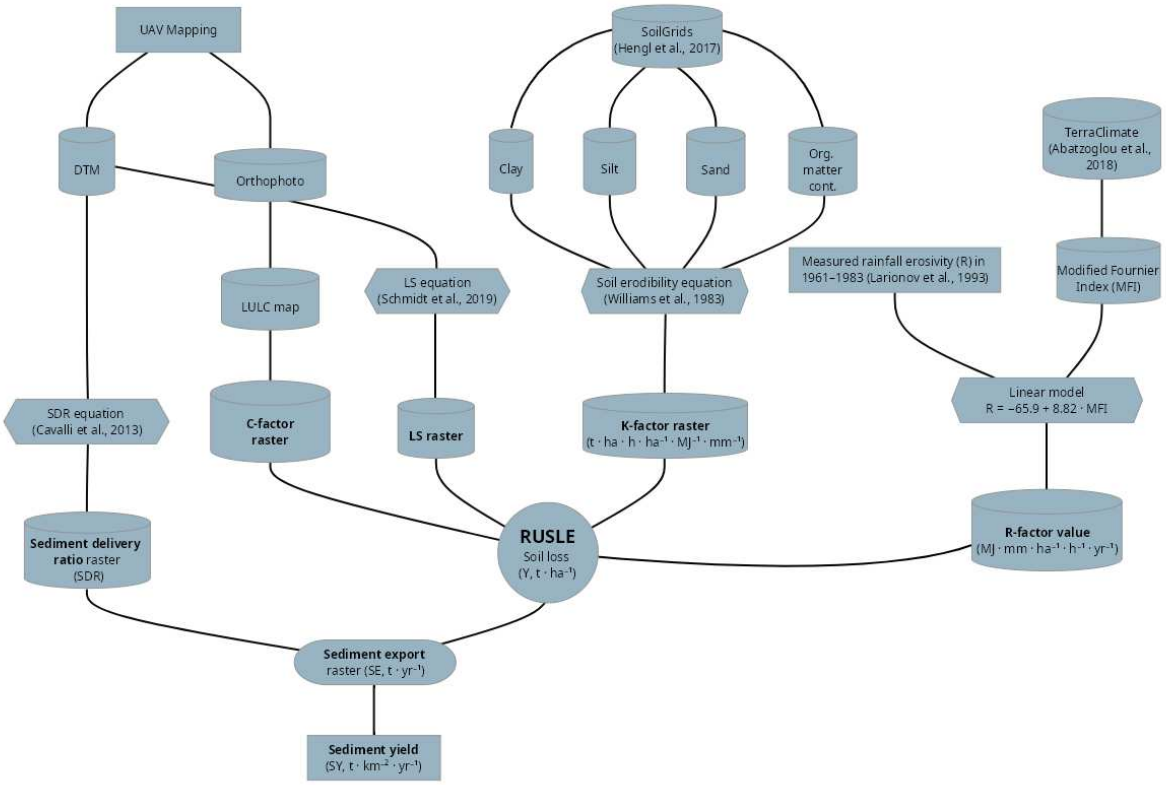

FIGURE 3. Here is a schematic outline of the methodological framework used to estimate the soil loss and sediment yield. Abbreviations and factors are explained in section 3.6 and supplementary material.

3.7 Statistical analysis

All reported confidence intervals (CI) were calculated as 95% credible (mean-centred quantile) intervals using a "ggdist" R package (Kay, 2022). All statistical analyses and GIS procedures were completed with R version 4.2 (R Core Team, 2022).

4. RESULTS

4.1 Volumetric sediment deposition rates and sediment yield

As of August 2020, the lake volume is 92 165 m^3 with a mean (SD) depth of 2.34 (1.0) m. Toward the lake centre, sediment thickness gradually decreases from the highest (1.5 m) near the inlet on the north (see Figure 2b). The sediment thickness has a mean (SD) of 0.41 (0.2) m. The total volume of lake deposits is 16 055 m^3. Considering the simulated dry bulk density of lake deposits, the total mass of accumulated deposits is 22 996 (95% CI, 13 214–31 344) tons with a mean annual sedimentation rate of 742 (95% CI, 426–1011) t yr^{-1} for 1989–2020. This resulted in a corresponding area-specific sediment yield (SY_{Lake}) of 403 (95% CI, 232–550) t km^{-2} yr^{-1}.

However, because we measured only the sediment layer potentially corresponding to the modern deposition period (i.e., since 2001; see Section 3.3 for details), the mean annual sedimentation rate should be 1150 (95% CI, 661–1567) t yr^{-1} with area-specific sediment yield of 625 (95% CI, 359–852) t km^{-2} yr^{-1} for 2001–2020 time frame. Therefore, considering the time uncertainty, by joining both distributions (1989–2020 and 2001–2020), we can assume that actual sediment yield lies in the 95% CI of 249–839 with a mean of 514 t km^{-2} yr^{-1}.

4.2 Sediment delivery ratio

The $SDR_{Cavalli}$ varied from 0.01 to 0.17 across the basin, with the average being 0.04 (95% CI, 0.015–0.126). In terms of spatial distribution, the higher $SDR_{Cavalli}$ values were recorded along the creek channel, lake, and low elevated areas (< 1300 m) in the south, while the lower values were recorded along the basin periphery and ridges (cf. Figure 4a). When calculating SDR manually, the mean SDR_{Manual} is equal to 0.041 with a narrow 95% CI (0.022–0.065) based on bulk density variability (see Sections 3.3 and 3.4).

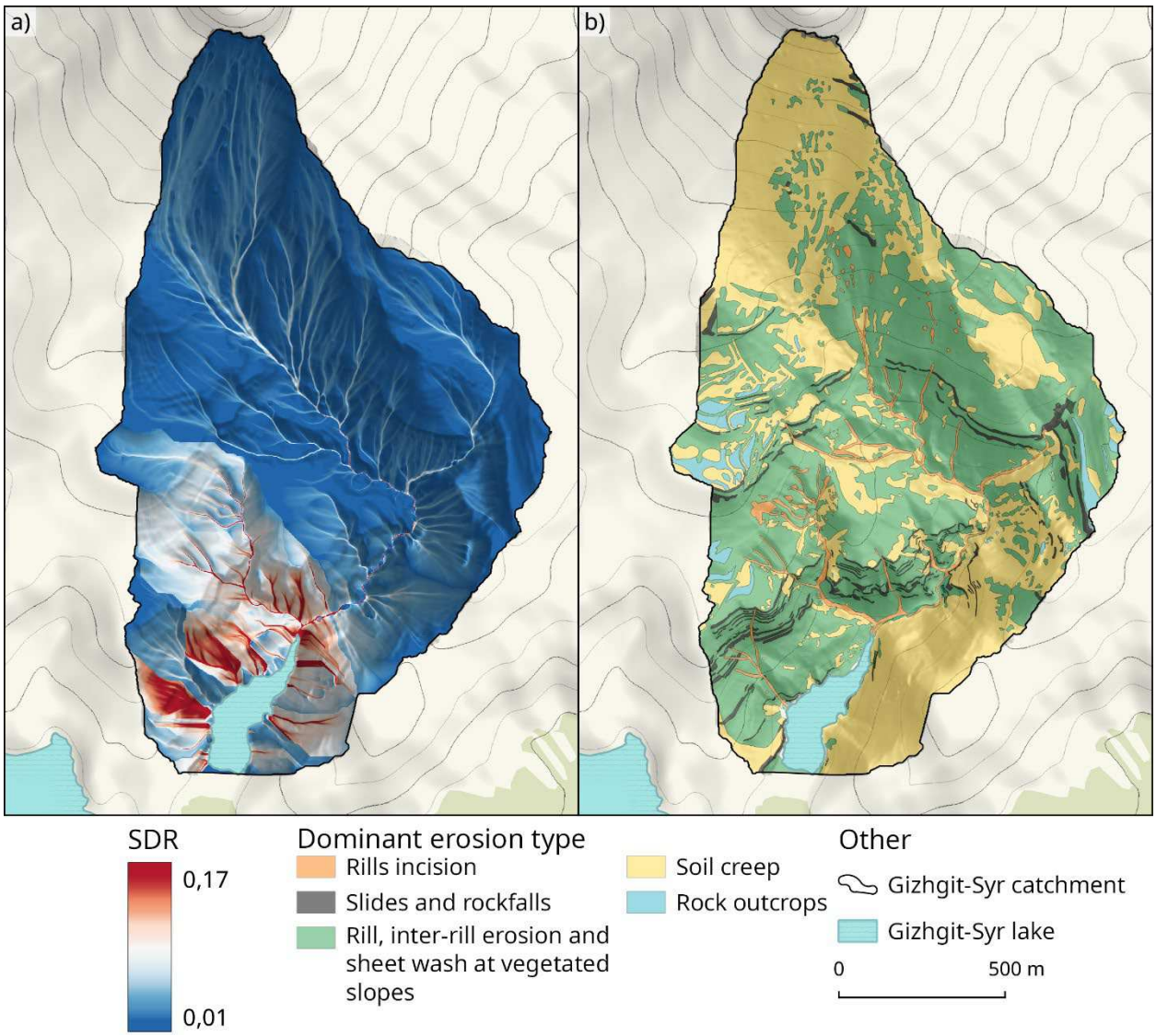

FIGURE 4. Sediment delivery ratio map (a) computed using Cavalli et al. (2013) approach; map of erosion types (b) digitised manually.

4.3 Erosion processes and sediment sources inventory

According to the map of erosion processes, the dominant erosion type (except soil creep) was sheet wash, covering 49% of the basin area. However, sheet erosion was responsible for only 26% of volumetric sediment loss, while soil creep removed almost half of all sediments (Table 2). Loss due to slides and rockfalls was 16%, and rill erosion was 9%. The gross sediment loss ($SL_{Erosion\ map}$) estimated using the anticipated mean annual erosion rates (see Table 1) was equal to 5971 t yr^{-1}. Estimated total volumetric sediment export (with $SDR_{Cavalli}$) was 258 m^3 yr^{-1}. Approximately 38% of this value is exported through sheet and rill erosion. In contrast, slides and rockfalls export 18% (see Table 2). After multiplying volumetric sediment losses by simulated bulk densities (see Section 3.5), the calculated sediment export ($SE_{Erosion\ map}$) was 787 (95% CI, 592–1005) t yr^{-1}. It corresponds to an area-specific sediment yield ($SY_{Erosion\ map}$) of 428 (95% CI, 322–546) t km^{-2} yr^{-1}.

TABLE 2. Summary statistics of estimated volumetric sediment loss and export from the Gizhgit-Syr catchment using mean erosion rates (see Table 1)

	Type of erosion process	Area, km^2	Estimate volumetric sediment loss, $m^3\ yr^{-1}$	Estimated volumetric sediment export (with $SDR_{Cavalli}$), $m^3\ yr^{-1}$	Percentage, %
1	Rills incision	0.051	566	32.3	12.5
2	Slides and rockfalls	0.051	938	46.1	17.9
3	Rill, inter-rill erosion and sheet wash at vegetated slopes	0.91	1577	64.7	25.1
4	Soil creep	0.76	2890	115	44.6
5	None	0.066	—	—	—
	Total	1.84	5971	258	100

4.4 RUSLE results

Figure 5c illustrates the spatial pattern of soil losses by sheet and rill erosion. It is mainly steep slopes that lead to strongly eroded areas in the northern and south-east part of the basin (LS-factor, Fig. 5b). We estimated the mean annual gross soil loss by RUSLE to be 3541 t yr^{-1}, with a mean (SD) soil loss rate of 19.4 (14.7) t ha^{-1} yr^{-1}.

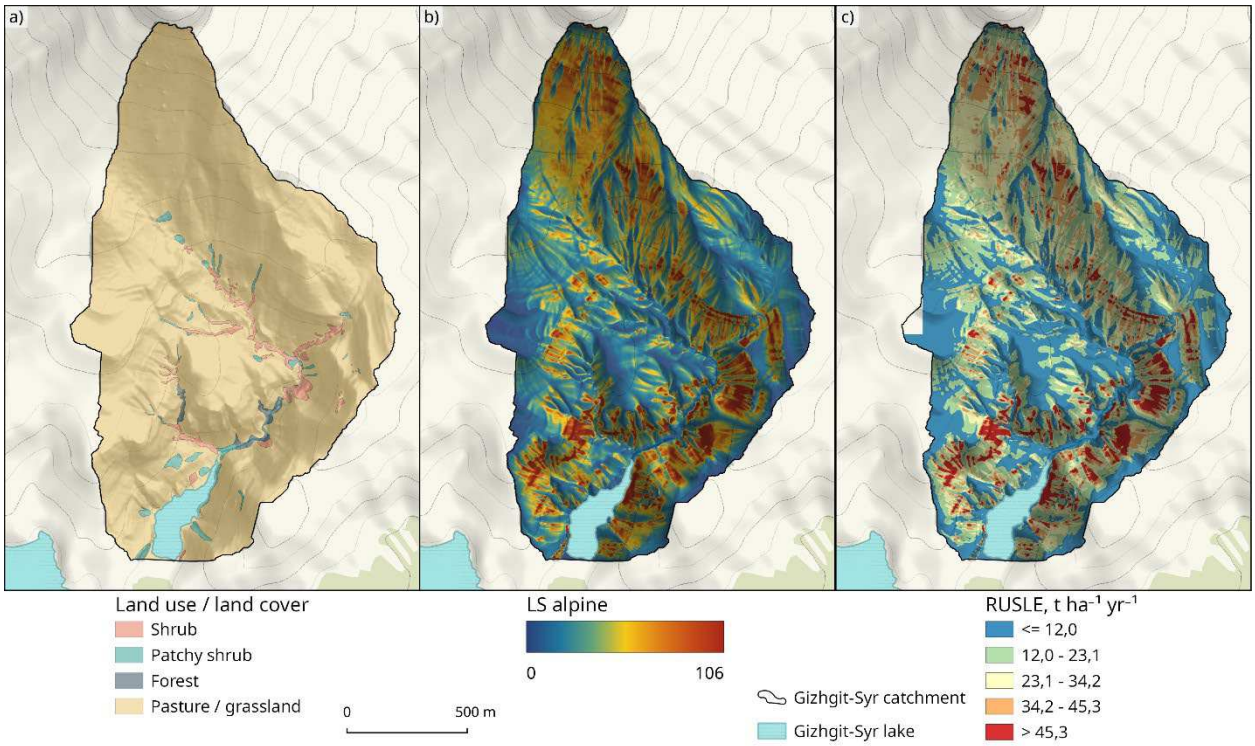

FIGURE 5. Land use / Land cover map of the Gizhgit-Syr catchment (a); LS_{alpine} map (b); potential soil loss due to rill and sheet erosion (RUSLE) map (c).

The mean rainfall erosivity for the 1989–2020 period was 807 (95% CI, 689–924) MJ mm ha $^{-1}$ h^{-1} yr^{-1}, considering the 95% confidence interval of the linear model (see Figure S6 and eq. S2). Taking into account the uncertainty in R-factor estimations and GIS-based sediment delivery ratios ($SDR_{Cavalli}$), the resulting sediment export by sheet and rill erosion for the 1989-2020 period (SE_{RUSLE}) equals 167 (95% CI, 142–191) t yr^{-1} with a corresponding area-specific value (SY_{RUSLE}) of 90.8 (95% CI, 77.2–104) t km^{-2} yr^{-1}.

5. DISCUSSION

There are three major findings in this study that help us understand sediment redistribution patterns in low mountainous areas. First, based on the lake sedimentation rate, we found that the mean annual area-specific sediment yield is 514 (95% CI, 249–839) t km^{-2} yr^{-1}. Similar results were obtained from the erosion mapping (i.e., a map of erosion processes) — 428 (95% CI, 322–546) t km^{-2} yr^{-1}. Secondly, the distribution of the erosion processes suggests that sheet and rill erosion exports *ca.* 25% of total sediment export, slides and rockfalls — 18%, while the rest is removed by soil creep. Thirdly, the RUSLE-based modelling of sheet wash and rill erosion has highlighted the areas most prone to water erosion. The corresponding mean annual soil erosion rate was very close to the results obtained from the literature review.

5.1 Erosion rates

Since we measured the sheet and rill erosion and rockfall over a short period, the data on their rates obtained during our observations do not reflect average long-term values. However, they can serve as estimates if compared to published data for the mountain ranges of the Alpide belt (Alewell et al., 2014; Anderson and Cox, 1978; Azhigirov and Golosov, 1990; Hales and Roering, 2005; Sass, 2007).

On average, rockfall processes in the Low and High Caucasus mountains do not exceed 3 cm yr^{-1} (Kharchenko et al., 2021). There is an average retreat rate of 0.2–0.7 cm yr^{-1} for sedimentary rock walls in the European Alps (Sass, 2007), whereas in the Southern Alps in New Zealand average 0.08–1.33 cm yr^{-1} (Hales and Roering, 2005). A slightly higher retreat rate for rock walls in Svalbard ranges from 0.33 to 1.96 mm yr^{-1} (Siewert et al., 2012). Based on the given values and our observations, we can conclude that rock walls retreat an average of 1.5 cm yr^{-1}.

The average annual rate of sheet erosion is difficult to estimate from the literature review since it depends on numerous factors, including slope length and steepness, grass projective cover, and rainfall intensity. For example, sheet erosion rates were between 0.7 and 2.1 mm yr^{-1} in the Western Caucasus (Bzugu River basin), where precipitation is up to 1500 mm yr^{-1} (Azhigirov, 1991). The average rate of sheet erosion in the Baikal depression was 1 mm yr^{-1} on slopes steeper than 20° but 7.3 mm yr^{-1} on slopes more vertical than 40° (Agafonov, 1985). Both catchments have slope lengths of approximately 300 m. In Gizhgit-Syr, the slope steepness is about 30° (see Table 1), while at the same time, the slope length is significantly lower due to the elongation of the catchment (cf. Figure 5b). Therefore, we expect that the

1.5 mm yr^{-1} rate used in our calculations reflects the average sheet erosion rate for the low mountain conditions.

According to our findings, the soil creep processes are responsible for almost half of sediment export. Directly the soil creep supplies only along the slope contact zone of the slow mass displacement soil and the lake. In the rest of the area, the creep only releases material for erosion. The displaced material a) is more mobile; b) is carried to the fast transit routes (Kirkby, 1967). Therefore, particles supplied by the soil creep to the fluvial network afterwards are involved in sediment export due to rill erosion. In addition, the erosion intensity may be greater than the supply of material by the creep, which not only removes the soil displaced by the creep but also incises and deepens the old erosional landforms.

The RUSLE-based soil erosion modelling suggested that mean soil loss rates for the whole Gizghit-Syr basin were 1.59 (95% CI, 1.36–1.82) mm yr^{-1}. At the same time, the maximum rates of 4.44 mm yr^{-1} were observed on slopes steeper than 40°. These rates correspond to the mean topsoil (0–30 cm) bulk density of 1.22 t m^{-3} derived from the SoilGrids database (Hengl et al., 2017) and RUSLE results described in Section 4.4. Given the assessment strategy, our results may differ from actual soil loss rates. However, our modelling results tend to be accurate as the 1970th study (Makkaveev, 1970) indicates that the mean annual soil erosion rate for the area of interest was 2 mm yr^{-1} with a maximum of 6 mm yr^{-1} for 1954–1969.

One may argue that we compared soil erosion rates obtained for various periods. We found a slight decrease in annual rainfall erosivity at −0.13 % yr^{-1} (Figure 6), but the Mann-Kendall test (Mann, 1945) didn't treat this decrease as significant (tau = −0.08, p-value =0.37). This suggests that since 1958 the denudation rate has remained the same, as we have identified. While it can't be excluded that grazing activity was higher before the collapse of the Soviet Union in 1991, it could have stimulated higher rates of sheet wash and rill erosion at that time.

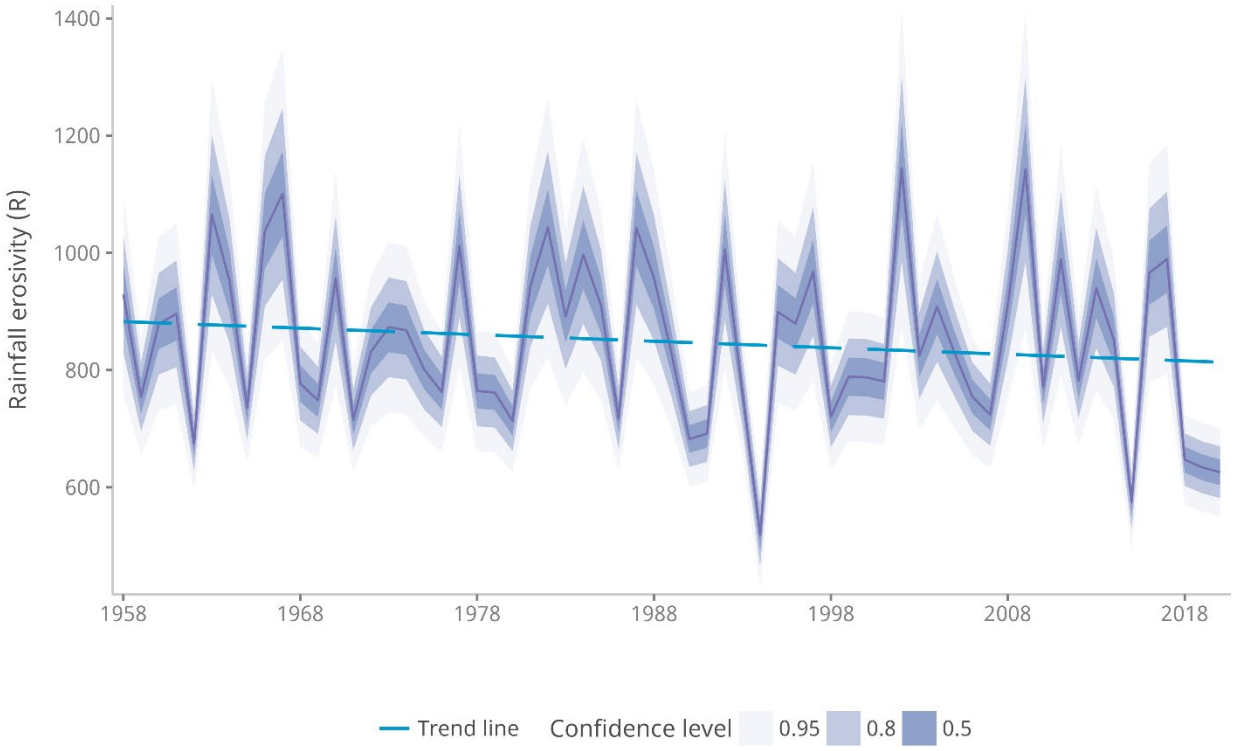

FIGURE 6. Rainfall erosivity time series for the Gizhgit-Syr catchment. The purple line displays the time series with the uncertainty envelope calculated with Eq. (S2). The blue line corresponds to a linear trend.

5.2 Sediment yield

Previous sediment yield studies in the Caucasus region were primarily based on gauging station measurements (e.g., Golosov and Tsyplenkov, 2021; Mozzherin and Sharifullin, 2015) or cosmogenic ^{10}Be concentrations (Forte et al., 2022). For example, a Tsyplenkov et al. (2019) study analysed area-specific sediment yields from 200 gages in the North and South Caucasus. According to their SY map of the Caucasus region, the weighted mean (SD) SY for the Gizhgit-Syr basin should be around 370 (130) t km^{-2} yr^{-1}. Our findings in this study mirror those results and others similarly focused on low mountain zones (e.g., Vanmaercke et al., 2011), but we estimated SY without direct gauging station measurements (see Table 3). However, values based on gauging station measurements alone tend to lower the sediment flux due to neglecting the bedload sediments (Vanmaercke et al., 2015). At the same time, the fraction of bedload material varies from river to river and can be up to 50% in mountain regions (Turowski et al., 2010). Vanmaercke et al. (2015) presented a logarithmic equation to predict the bedload fraction (f_{BL}, %) from the catchment area (A, km^2):

$$f_{BL} = 0.45 - 0.04 \cdot \ln A, \quad (12)$$

According to Eq. 12, the bedload fraction for the 1.84 km^2 Gizhgit-Syr basin should be 43% of the total sediment load. It follows that the total sediment yield should be *ca.* 528 t km^{-2} yr^{-1} based on the map from Tsyplenkov et al. (2019). Contrariwise, erosion rates obtained from cosmogenic radionuclides (Forte et al., 2022) suggest tenfold lower values. Thus, using the relationship between the mean basin gradient and the erosion

rate presented in their study, we can roughly estimate the mean erosion rate of 200 m Myr^{-1} with a mean basin gradient of 0.5 m m^{-1}.

Considering the dominant erosion processes ratio (see Table 2), the sheet and rill erosion is responsible for 25% of total sediment export. Using this ratio, we can roughly assess the total sediment yield ($\widehat{SY_{RUSLE}}$, t km^{-2} yr^{-1}) using only RUSLE estimates by multiplying SY_{RUSLE} by four. Such assessment is feasible because the SY_{RUSLE} is the area-specific sediment yield caused only by sheet and rill erosion.

Consequently, various SY estimation approaches give similar results (see Table 3), especially since the 95% confidence intervals overlap. Given the uncertainty of the lake sediment deposition period and other uncertainties (see Section 5.4 for details), the SY may vary from 232 to 839 t km^{-2} yr^{-1}. However, it seems to us that the SY_{Lake} with a 95% CI of 249–839 and mean of 514 t km^{-2} yr^{-1}, accounts for all uncertainties and best approximates reality. A recent study (Hinderer et al., 2013) from small basins (A < 500 km^2) of the Northern and Southern Alps reported a mean annual sediment yield of 465 and 557 t km^{-2} $yr^{-1,}$ respectively. Even though the sediment deposition rates in small low-mountain Alpine lakes slightly increased in Anthropocene (Rose et al., 2011), our estimate indicates the same order of magnitude.

TABLE 3. Comparison of various methods used in the present study to assess the area-specific sediment yield (SY, t km^{-2} yr^{-1}). The mean, lower and upper bounds of 95 % CI are presented.

Method	Period	Mean	Lower bound	Upper bound	Source
SY_{Lake}	1989–2020	403	232	550	This study. See Section 4.1 for details
	2001–2020	625	359	852	This study. See Section 4.1 for details
	All	514	249	839	This study. See Section 4.1 for details
$SY_{Erosion\ map}$	2020–2021	428	322	546	This study. See Section 4.3 for details
SY_{RUSLE}	1989–2020	90.8	77.2	104	This study. See Section 4.4 for details
$\widehat{SY_{RUSLE}}$	1989–2020	363	309	416	This study. See Section 5.2 for details
Gauging station measurements	*ca.* 1925–2015	370	—	—	(Tsyplenkov et al., 2019)
Gauging station measurements with bedload model	*ca.* 1925–2015	528	—	—	(Tsyplenkov et al., 2019; Vanmaercke et al., 2015)

5.3 Sediment delivery

We can also validate our results by comparing the $SDR_{Cavalli}$ and SDR_{Manual} distributions (see Fig.7). We previously reported that mean SDR values computed with various methods are close and equal to *ca.* 0.04. However, the variability of $SDR_{Cavalli}$ is higher than SDR_{Manual}, even when accounting for almost all possible dry bulk densities (see Section 3.5). Nevertheless, the Student's t-test for samples with unequal and unknown variances suggests that both SDR belongs to the same distribution (t = 2.86, p-value = 0.9). The SDR of 0.04 is very close to global estimates for small catchments and hillslopes of mountain areas. Thus, a 2018th study from the Austrian Central Alps reports a mean SDR of *ca.* 0.06 (Heckmann and Vericat, 2018). In comparison, a more detailed analysis from the Ötztal Alps (Hilger et al., 2019) suggests that SDR significantly varies between processes, with a mean basin SDR of 0.026. Despite their uncertainties, these values provide an independent measure of the approach used in this study, particularly regarding soil loss and sediment transport.

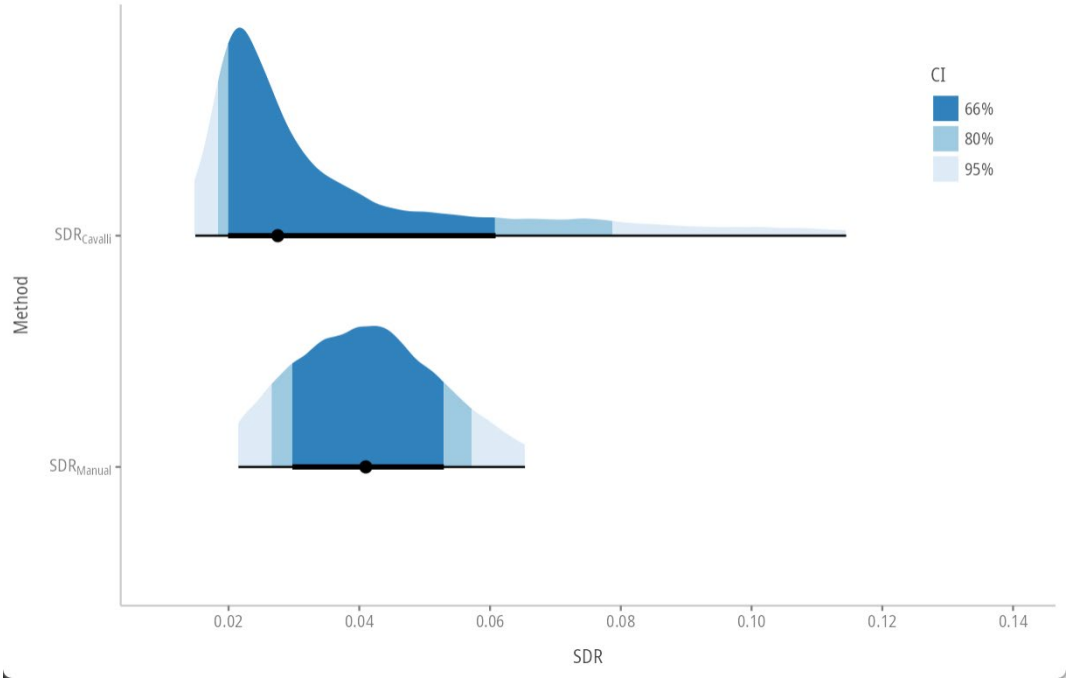

FIGURE 7. SDR values are computed using various methods.

5.4 Uncertainty assessment and further implications

Studies conducted in ungauged basins are usually subject to many uncertainties (Hrachowitz et al., 2013). It is the case with our research as well. We tried to consider many factors, but there are still some areas where the results could have been significantly affected.

One of the major limitations of our research is the absence of bottom sediment density, which increases the sedimentation rate variability. Previous studies have highlighted sediment density's importance in sediment transport modelling (Hostache et al., 2014; Lepesqueur et al., 2019). The uncertainty assessment approach suggested by Reinwarth et al. (2019) should be used in future studies to precisely evaluate sediment yield derived from volumetric sediment deposition rates.

The equipment used for the lake bathymetry survey (Deeper Chirp+) has a low-quality built-in GPS receiver with an expected accuracy of up to several meters. Previously, a study showed that horizontal errors could reach 30 meters (Bandini et al., 2018). However, they used an older model (Deeper PRO+) that only used GPS satellites. The current model uses GPS, GLONASS, Galileo, BeiDou, and QZSS to locate itself. Therefore, it is expected that the positioning precision should be higher. However, we didn't assess it.

Due to a limited number of stations with measured rainfall erosivity (rainfall intensity at least) in the study region, we had to use only eight stations to create a linear model (see Supporting Information). This number of points is certainly not enough to build a robust model, and including additional stations may seriously alter the relationship. Moreover, the 2009 study revealed that Modified Fournier Index is inappropriate for predicting rainfall erosivity (Angulo-Martínez and Beguería, 2009) and should not be used. However, there is no significant difference in rainfall erosivity estimated for the whole world by Panagos et al. (2017) and our study. The mean annual rainfall erosivity for 1961–1983 for the Gizhgit-Syr catchment is 730±133 (Panagos et al., 2017), while our assessment (Eq. S2) indicates that for that period, rainfall erosivity should be 868±143 MJ mm ha $^{-1}$ h^{-1} yr^{-1}. Considering the overlapping 95% confidence intervals, the difference is not significant.

CONCLUSION

Three major conclusions were drawn from our study of sediment transport in the small low mountain Gizhgit-Syr basin of the Northern Caucasus. First, we defined the mean annual area-specific sediment yield using various independent methods. Lake sediment deposition rate, erosion mapping and soil erosion modelling suggest similar results of 514 (95% CI, 249–839) t km^{-2} yr^{-1}. This finding is consistent with those for other low mountain catchments of the Alpide belt. Secondly, the erosion mapping (i.e., a map of erosion processes) revealed that sheet and rill erosion is responsible for *ca.* 40% of total sediment export, slides and rockfalls — 18%, while the rest is removed by soil creep. Even soil creep does not export sediments directly to the fluvial network; it plays a crucial role in detachment processes. Additionally, the RUSLE-based modelling of sheet wash and rill erosion has highlighted the areas most prone to soil erosion. The corresponding mean annual soil erosion rate of 1.59 mm yr^{-1} was very close to the results obtained from the literature review.

The sediment delivery ratio comparison also validated the reliability of our results. Both manually calculated and DEM-based approaches suggested a mean SDR of 0.04. The SDR map shows that almost half of the catchment has very low SDR values and is mainly not involved in sediment transport. This fact is endorsed by the visual inspection of the Gizhgit-Syr valley: a poorly incised temporary watercourse runs along the bottom of the valley, with woody and shrub vegetation without evidence of flooding.

By identifying the dominant erosion processes and rates, this study will contribute to maintaining and sustainably managing the low-elevation grasslands that are vital to North Caucasus agriculture by identifying the main

707 erosion processes contributing to sediment yield in the representative
708 catchment for that region.
709

710 **REFERENCES**

711 Agafonov BP. 1985. Sheet erosion in the Baikal depression. Geomorfologiya :
712 29–36.

713 Alewell C, Meusburger K, Juretzko G, Mabit L, Ketterer ME. 2014. Suitability
714 of 239+240Pu and 137Cs as tracers for soil erosion assessment in mountain
715 grasslands. Chemosphere **103** : 274–280. DOI:
716 10.1016/j.chemosphere.2013.12.016

717 Alexandrin MY, Darin AV, Kalugin IA, Dolgova EA, Grachev AM, Solomina ON.
718 2018. Annual Sedimentary Record From Lake Donguz-Orun (Central
719 Caucasus) Constrained by High Resolution SR-XRF Analysis and Its Potential
720 for Climate Reconstructions. Frontiers in Earth Science **6** [online] Available
721 from: https://www.frontiersin.org/article/10.3389/feart.2018.00158
722 (Accessed 17 February 2022)

723 Anderson EW, Cox NJ. 1978. A comparison of different instruments for
724 measuring soil creep. CATENA **5** : 81–93. DOI: 10.1016/0341-
725 8162(78)90001-2

726 Andrushhuk VL, Dubinsky AYa, Hain BE (eds). 1968. Geology of the USSR.
727 Vol. 9. The Northern Caucasus. Part 1. Geological description. . Nedra:
728 Moscow

729 Angulo-Martínez M, Beguería S. 2009. Estimating rainfall erosivity from daily
730 precipitation records: A comparison among methods using data from the Ebro
731 Basin (NE Spain). Journal of Hydrology **379** : 111–121. DOI:
732 10.1016/j.jhydrol.2009.09.051

733 Azhigirov AA. 1991. On the significance of various erosion processes in
734 slope evolution at the NW Caucasus. Geomorphology RAS : 46–51.

735 Azhigirov AA, Golosov VN. 1990. Slow mass movement assessment in
736 engineering-geographical studies. Geomorphology RAS : 33–40.

737 Bandini F, Olesen D, Jakobsen J, Kittel CMM, Wang S, Garcia M, Bauer-
738 Gottwein P. 2018. Technical note: Bathymetry observations of inland water
739 bodies using a tethered single-beam sonar controlled by an unmanned aerial
740 vehicle. Hydrology and Earth System Sciences **22** : 4165–4181. DOI:
741 10.5194/hess-22-4165-2018

742 Batista PVG, Laceby JP, Davies J, Carvalho TS, Tassinari D, Silva MLN, Curi N,
743 Quinton JN. 2021. A framework for testing large-scale distributed soil erosion
744 and sediment delivery models: Dealing with uncertainty in models and the
745 observational data. Environmental Modelling & Software **137** : 104961. DOI:
746 10.1016/j.envsoft.2021.104961

747 Bircher P, Liniger HP, Prasuhn V. 2019. Comparing different multiple flow
748 algorithms to calculate RUSLE factors of slope length (L) and slope steepness
749 (S) in Switzerland. Geomorphology **346** : 106850. DOI:
750 10.1016/j.geomorph.2019.106850

751 Blake WH et al. 2018. A deconvolutional Bayesian mixing model approach for
752 river basin sediment source apportionment. Scientific Reports **8** : 13073. DOI:
753 10.1038/s41598-018-30905-9

754 Borrelli P et al. 2021. Soil erosion modelling: A global review and statistical
755 analysis. Science of The Total Environment : 146494. DOI:
756 10.1016/j.scitotenv.2021.146494

757 Borselli L, Cassi P, Torri D. 2008. Prolegomena to sediment and flow
758 connectivity in the landscape: A GIS and field numerical assessment. CATENA
759 **75** : 268–277. DOI: 10.1016/j.catena.2008.07.006

760 Bortnikov NS, Gurbanov AG, Dokuchaev AY, Bortnikov NS, Gurbanov AG,
761 Dokuchaev AY. 2020. Tailing dumps of the tyrnyauz tungsten–molybdenum
762 mining and processing complex: Current state and outlooks. Global Journal of
763 Ecology **5** : 088–092. DOI: 10.17352/gje.000025

764 Buachidze IM, Dzhandzhgava KI, Churinova MV (eds). 1978. Engineering
765 geology of USSR. Vol. 8. Caucasus, Crimea, Carpathians . Izd. Moskovskogo
766 univ: Moskva

767 Carrillo R, Mao L. 2020. Coupling Sediment Transport Dynamics with Sediment
768 and Discharge Sources in a Glacial Andean Basin. Water **12** : 3452. DOI:
769 10.3390/w12123452

770 Cavalli M, Marchi L. 2008. Characterisation of the surface morphology of an
771 alpine alluvial fan using airborne LiDAR. Natural Hazards and Earth System
772 Sciences **8** : 323–333. DOI: 10.5194/nhess-8-323-2008

773 Cavalli M, Tarolli P, Marchi L, Dalla Fontana G. 2008. The effectiveness of
774 airborne LiDAR data in the recognition of channel-bed morphology. CATENA
775 **73** : 249–260. DOI: 10.1016/j.catena.2007.11.001

776 Cavalli M, Trevisani S, Comiti F, Marchi L. 2013. Geomorphometric assessment
777 of spatial sediment connectivity in small Alpine catchments. Geomorphology
778 **188** : 31–41. DOI: 10.1016/j.geomorph.2012.05.007

779 Crema S, Cavalli M. 2018. SedInConnect: a stand-alone, free and open source
780 tool for the assessment of sediment connectivity. Computers & Geosciences
781 **111** : 39–45. DOI: 10.1016/j.cageo.2017.10.009

782 Dethier EN, Renshaw CE, Magilligan FJ. 2022. Rapid changes to global river
783 suspended sediment flux by humans. Science **376** : 1447–1452. DOI:
784 10.1126/science.abn7980

Forte AM, Leonard JS, Rossi MW, Whipple KX, Heimsath AM, Sukhishvili L, Godoladze T, Kadirov F. 2022. Low variability runoff inhibits coupling of climate, tectonics, and topography in the Greater Caucasus. Earth and Planetary Science Letters **584** : 117525. DOI: 10.1016/j.epsl.2022.117525

Forte AM, Whipple KX, Bookhagen B, Rossi MW. 2016. Decoupling of modern shortening rates, climate, and topography in the Caucasus. Earth and Planetary Science Letters **449** : 282–294. DOI: 10.1016/j.epsl.2016.06.013

Funk C et al. 2015. The climate hazards infrared precipitation with stations—a new environmental record for monitoring extremes. Scientific Data **2** : 150066. DOI: 10.1038/sdata.2015.66

Garrison E. 2016. Techniques for Archaeological Sediments and Soils. In Techniques in Archaeological Geology , Garrison E (ed). Springer International Publishing: Cham; 77–113. [online] Available from: https://doi.org/10.1007/978-3-319-30232-4_4 (Accessed 22 June 2022)

Gitelson AA, Kaufman YJ, Stark R, Rundquist D. 2002. Novel algorithms for remote estimation of vegetation fraction. Remote Sensing of Environment **80** : 76–87. DOI: 10.1016/S0034-4257(01)00289-9

Golosov V, Tsyplenkov A. 2021. Factors Controlling Contemporary Suspended Sediment Yield in the Caucasus Region. Water **13** : 3173. DOI: 10.3390/w13223173

Govers G. 2010. Misapplications and Misconceptions of Erosion Models. In Handbook of Erosion Modelling , . John Wiley & Sons, Ltd; 117–134. [online] Available from: https://onlinelibrary.wiley.com/doi/abs/10.1002/9781444328455.ch7 (Accessed 26 June 2022)

Hadley RF, Walling DE, Elwell HA (eds). 1984. Erosion and sediment yield: some methods of measurement and modelling . Geo Books: Norwich, England

Hales TC, Roering JJ. 2005. Climate-controlled variations in scree production, Southern Alps, New Zealand. Geology **33** : 701. DOI: 10.1130/G21528.1

Hasholt B, Walling DE, Owens PN. 2000. Sedimentation in arctic proglacial lakes: Mittivakkat Glacier, south-east Greenland. Hydrological Processes **14** : 679–699. DOI: https://doi.org/10.1002/(SICI)1099-1085(200003)14:4<679::AID-HYP966>3.0.CO;2-E

Heckmann T, Hilger L, Vehling L, Becht M. 2016. Integrating field measurements, a geomorphological map and stochastic modelling to estimate the spatially distributed rockfall sediment budget of the Upper Kaunertal, Austrian Central Alps. Geomorphology **260** : 16–31. DOI: 10.1016/j.geomorph.2015.07.003

Heckmann T, Schwanghart W. 2013. Geomorphic coupling and sediment connectivity in an alpine catchment — Exploring sediment cascades using

graph theory. Geomorphology **182** : 89–103. DOI: 10.1016/j.geomorph.2012.10.033

Heckmann T, Vericat D. 2018. Computing spatially distributed sediment delivery ratios: inferring functional sediment connectivity from repeat high-resolution digital elevation models. Earth Surface Processes and Landforms **43** : 1547–1554. DOI: 10.1002/esp.4334

Hengl T et al. 2017. SoilGrids250m: Global gridded soil information based on machine learning. PLOS ONE **12** : e0169748. DOI: 10.1371/journal.pone.0169748

Hilger L et al. 2019. A Sediment Budget of the Upper Kaunertal. In Geomorphology of Proglacial Systems: Landform and Sediment Dynamics in Recently Deglaciated Alpine Landscapes , Heckmann T and Morche D (eds). Springer International Publishing: Cham; 289–312. [online] Available from: https://doi.org/10.1007/978-3-319-94184-4_17 (Accessed 21 September 2021)

Hinderer M, Kastowski M, Kamelger A, Bartolini C, Schlunegger F. 2013. River loads and modern denudation of the Alps — A review. Earth-Science Reviews **118** : 11–44. DOI: 10.1016/j.earscirev.2013.01.001

Holland EC. 2016. Economic Development and Subsidies in the North Caucasus. Problems of Post-Communism **63** : 50–61. DOI: 10.1080/10758216.2015.1067750

Hostache R, Hissler C, Matgen P, Guignard C, Bates P. 2014. Modelling suspended-sediment propagation and related heavy metal contamination in floodplains: a parameter sensitivity analysis. Hydrology and Earth System Sciences **18** : 3539–3551. DOI: 10.5194/hess-18-3539-2014

Hovsepyan R. 2015. On the agriculture and vegetal food economy of Kura-Araxes culture in the South Caucasus. Paléorient **41** : 69–82. DOI: 10.3406/paleo.2015.5656

Hrachowitz M et al. 2013. A decade of Predictions in Ungauged Basins (PUB)—a review. Hydrological Sciences Journal **58** : 1198–1255. DOI: 10.1080/02626667.2013.803183

Ivanov MM, Konoplev AV, Walling DE, Konstantinov EA, Gurinov AL, Ivanova NN, Kuzmenkova NV, Tsyplenkov AS, Ivanov MA, Golosov VN. 2021. Using reservoir sediment deposits to determine the longer-term fate of chernobyl-derived 137Cs fallout in the fluvial system. Environmental Pollution **274** : 116588. DOI: 10.1016/j.envpol.2021.116588

Ivanov MM, Kuzmenkova NV, Rozhkova AK, Grabenko EA, Grachev AM, Golosov VN. 2022. The anthropogenic fallout radionuclides in soils of Mount Khuko (the Western Caucasus) and their application for determination of sediment redistribution. Journal of Environmental Radioactivity **248** : 106880. DOI: 10.1016/j.jenvrad.2022.106880

Kay M. 2022. ggdist: Visualizations of Distributions and Uncertainty [online] Available from: https://mjskay.github.io/ggdist/

Kharchenko SV, Fedin AV, Golosov VN. 2021. Denudation rates in the mountain periglacial regions: research methods and results. Geomorphology RAS **52** : 3–18. DOI: 10.31857/S0435428121010065

Kirkby MJ. 1967. Measurement and Theory of Soil Creep. The Journal of Geology **75** : 359–378. DOI: 10.1086/627267

Lepesqueur J, Hostache R, Martínez-Carreras N, Montargès-Pelletier E, Hissler C. 2019. Sediment transport modelling in riverine environments: on the importance of grain-size distribution, sediment density, and suspended sediment concentrations at the upstream boundary. Hydrology and Earth System Sciences **23** : 3901–3915. DOI: 10.5194/hess-23-3901-2019

Lewińska KE, Buchner J, Bleyhl B, Hostert P, Yin H, Kuemmerle T, Radeloff VC. 2021. Changes in the grasslands of the Caucasus based on Cumulative Endmember Fractions from the full 1987–2019 Landsat record. Science of Remote Sensing **4** : 100035. DOI: 10.1016/j.srs.2021.100035

Makkaveev NI (ed). 1970. Soil erosion and debris flows in Kabardino-Balkar republic . Nalchik

Mann HB. 1945. Nonparametric Tests Against Trend. Econometrica **13** : 245. DOI: 10.2307/1907187

Messenzehl K, Hoffmann T, Dikau R. 2014. Sediment connectivity in the high-alpine valley of Val Müschauns, Swiss National Park — linking geomorphic field mapping with geomorphometric modelling. Geomorphology **221** : 215–229. DOI: 10.1016/j.geomorph.2014.05.033

Meusburger K, Alewell C. 2008. Impacts of anthropogenic and environmental factors on the occurrence of shallow landslides in an alpine catchment (Urseren Valley, Switzerland). Natural Hazards and Earth System Sciences **8** : 509–520. DOI: 10.5194/nhess-8-509-2008

Mills K et al. 2017. Deciphering long-term records of natural variability and human impact as recorded in lake sediments: a palaeolimnological puzzle. WIREs Water **4** : e1195. DOI: 10.1002/wat2.1195

Mozzherin VV, Sharifullin AG. 2015. Estimation of current denudation rate of the mountains based on the suspended sediment runoff of the rivers (the Tien Shan, the Pamir-Alai, the Caucasus, and the Alps as an example). Geomorphology RAS : 15–23. DOI: 10.15356/0435-4281-2014-1-15-23

Mücher CA, Wascher DM, Klijn JA, Koomen AJM, Jongman RHG. 2006. A new European landscape map as an integrative framework for landscape character assessment. 233–243 pp.

Najafi S, Dragovich D, Heckmann T, Sadeghi SH. 2021. Sediment connectivity concepts and approaches. CATENA **196** : 104880. DOI: 10.1016/j.catena.2020.104880

Navas A, Lizaga I, Gaspar L, Latorre B, Dercon G. 2020. Unveiling the provenance of sediments in the moraine complex of Aldegonda Glacier (Svalbard) after glacial retreat using radionuclides and elemental fingerprints. Geomorphology **367** : 107304. DOI: 10.1016/j.geomorph.2020.107304

Panagos P et al. 2017. Global rainfall erosivity assessment based on high-temporal resolution rainfall records. Scientific Reports **7** : 4175. DOI: 10.1038/s41598-017-04282-8

Perov V, Chernomorets S, Budarina O, Savernyuk E, Leontyeva T. 2017. Debris flow hazards for mountain regions of Russia: regional features and key events. Natural Hazards **88** : 199–235. DOI: 10.1007/s11069-017-2841-3

Pismenny AN, Tereshhenko VV, Marchenko RV, Popov SA, Tereshhenko LA, Prokuronov PV, Markus MA. 2021. State Geological Map of the Russian Federation. Scale 1 : 200 000. Second edition. Series Caucasian. Sheet K-38-II (Nalchik).

Pool S, Viviroli D, Seibert J. 2017. Prediction of hydrographs and flow-duration curves in almost ungauged catchments: Which runoff measurements are most informative for model calibration? Journal of Hydrology **554** : 613–622. DOI: 10.1016/j.jhydrol.2017.09.037

R Core Team. 2022. R: A Language and Environment for Statistical Computing . R Foundation for Statistical Computing: Vienna, Austria [online] Available from: https://www.R-project.org/

Reinwarth B, Petersen R, Baade J. 2019. Inferring mean rates of sediment yield and catchment erosion from reservoir siltation in the Kruger National Park, South Africa: An uncertainty assessment. Geomorphology **324** : 1–13. DOI: 10.1016/j.geomorph.2018.09.007

Renard KG, Agricultural Research Service W, Foster GR, Weesies GA, McCool DK, Yoder DC. 1997. Predicting soil erosion by water: a guide to conservation planning with the Revised Universal Soil Loss Equation (RUSLE) [online] Available from: https://agris.fao.org/agris-search/search.do?recordID=XF2015047686 (Accessed 19 April 2021)

Rets EP, Durmanov IN, Kireeva MB, Smirnov AM, Popovnin VV. 2020. Past' peak water' in the North Caucasus: deglaciation drives a reduction in glacial runoff impacting summer river runoff and peak discharges. Climatic Change DOI: 10.1007/s10584-020-02931-y [online] Available from: https://doi.org/10.1007/s10584-020-02931-y (Accessed 5 December 2020)

Richardson DC et al. 2022. A functional definition to distinguish ponds from lakes and wetlands. Scientific Reports **12** : 10472. DOI: 10.1038/s41598-022-14569-0

945 Rose NL, Morley D, Appleby PG, Battarbee RW, Alliksaar T, Guilizzoni P,
946 Jeppesen E, Korhola A, Punning J-M. 2011. Sediment accumulation rates in
947 European lakes since AD 1850: trends, reference conditions and exceedence.
948 Journal of Paleolimnology **45** : 447–468. DOI: 10.1007/s10933-010-9424-6

949 Sass O. 2007. Bedrock detection and talus thickness assessment in the
950 European Alps using geophysical methods. Journal of Applied Geophysics **62**
951 : 254–269. DOI: 10.1016/j.jappgeo.2006.12.003

952 Schillereff DN, Chiverrell RC, Macdonald N, Hooke JM. 2014. Flood
953 stratigraphies in lake sediments: A review. Earth-Science Reviews **135** : 17–
954 37. DOI: 10.1016/j.earscirev.2014.03.011

955 Siewert MB, Krautblatter M, Christiansen HH, Eckerstorfer M. 2012. Arctic
956 rockwall retreat rates estimated using laboratory-calibrated ERT
957 measurements of talus cones in Longyeardalen, Svalbard: ROCKWALL
958 RETREAT IN LONGYEARDALEN. Earth Surface Processes and Landforms **37** :
959 1542–1555. DOI: 10.1002/esp.3297

960 Soloviev SG, Kryazhev SG, Dvurechenskaya SS, Kryazhev VS, Emkuzhev MS,
961 Bortnikov NS. 2021. The superlarge Tyrnyauz skarn W-Mo and stockwork Mo(-
962 W) to Au(-Mo, W, Bi, Te) deposit in the Northern Caucasus, Russia: Geology,
963 geochemistry, mineralization, and fluid inclusion characteristics. Ore Geology
964 Reviews **138** : 104384. DOI: 10.1016/j.oregeorev.2021.104384

965 Syvitski J, Ángel JR, Saito Y, Overeem I, Vörösmarty CJ, Wang H, Olago D.
966 2022. Earth's sediment cycle during the Anthropocene. Nature Reviews Earth
967 & Environment **3** : 179–196. DOI: 10.1038/s43017-021-00253-w

968 Toropov PA, Aleshina MA, Grachev AM. 2019. Large-scale climatic factors
969 driving glacier recession in the Greater Caucasus, 20th–21st century.
970 International Journal of Climatology **39** : 4703–4720. DOI:
971 https://doi.org/10.1002/joc.6101

972 Tsyplenkov A, Vanmaercke M, Collins AL, Kharchenko S, Golosov V. 2021a.
973 Elucidating suspended sediment dynamics in a glacierized catchment after an
974 exceptional erosion event: The Djankuat catchment, Caucasus Mountains,
975 Russia. CATENA **203** : 105285. DOI: 10.1016/j.catena.2021.105285

976 Tsyplenkov A, Vanmaercke M, Golosov V. 2019. Contemporary suspended
977 sediment yield of Caucasus mountains. Proceedings of the International
978 Association of Hydrological Sciences **381** : 87–93. DOI: 10.5194/piahs-381-
979 87-2019

980 Tsyplenkov AS, Golosov VN, Belyakova PA. 2021b. How did the suspended
981 sediment load change in the North Caucasus during the Anthropocene?
982 Hydrological Processes **35** : 1–20. DOI: 10.1002/hyp.14403

983 Turowski JM, Rickenmann D, Dadson SJ. 2010. The partitioning of the total
984 sediment load of a river into suspended load and bedload: a review of

empirical data. Sedimentology **57** : 1126–1146. DOI: 10.1111/j.1365-3091.2009.01140.x

Vanmaercke M, Poesen J, Broeckx J, Nyssen J. 2014. Sediment yield in Africa. Earth-Science Reviews **136** : 350–368. DOI: 10.1016/j.earscirev.2014.06.004

Vanmaercke M, Poesen J, Govers G, Verstraeten G. 2015. Quantifying human impacts on catchment sediment yield: A continental approach. Global and Planetary Change **130** : 22–36. DOI: 10.1016/j.gloplacha.2015.04.001

Vanmaercke M, Poesen J, Radoane M, Govers G, Ocakoglu F, Arabkhedri M. 2012. How long should we measure? An exploration of factors controlling the inter-annual variation of catchment sediment yield. Journal of Soils and Sediments **12** : 603–619. DOI: 10.1007/s11368-012-0475-3

Vanmaercke M, Poesen J, Verstraeten G, de Vente J, Ocakoglu F. 2011. Sediment yield in Europe: Spatial patterns and scale dependency. Geomorphology **130** : 142–161. DOI: 10.1016/j.geomorph.2011.03.010

de Vente J, Poesen J, Verstraeten G, Govers G, Vanmaercke M, Van Rompaey A, Arabkhedri M, Boix-Fayos C. 2013. Predicting soil erosion and sediment yield at regional scales: Where do we stand? Earth-Science Reviews **127** : 16–29. DOI: 10.1016/j.earscirev.2013.08.014

Verstraeten G, Poesen J. 2000. Estimating trap efficiency of small reservoirs and ponds: methods and implications for the assessment of sediment yield. Progress in Physical Geography: Earth and Environment **24** : 219–251. DOI: 10.1177/030913330002400204

Verstraeten G, Poesen J. 2001a. The importance of sediment characteristics and trap efficiency in assessing sediment yield using retention ponds. Physics and Chemistry of the Earth, Part B: Hydrology, Oceans and Atmosphere **26** : 83–87. DOI: 10.1016/S1464-1909(01)85019-X

Verstraeten G, Poesen J. 2001b. Variability of dry sediment bulk density between and within retention ponds and its impact on the calculation of sediment yields. Earth Surface Processes and Landforms **26** : 375–394. DOI: 10.1002/esp.186

Verstraeten G, Poesen J. 2002. Using sediment deposits in small ponds to quantify sediment yield from small catchments: possibilities and limitations. Earth Surface Processes and Landforms **27** : 1425–1439. DOI: 10.1002/esp.439

Vezzoli G, Garzanti E, Limonta M, Radeff G. 2020. Focused erosion at the core of the Greater Caucasus: Sediment generation and dispersal from Mt. Elbrus to the Caspian Sea. Earth-Science Reviews **200** : 102987. DOI: 10.1016/j.earscirev.2019.102987

1024 Vigiak O, Borselli L, Newham LTH, McInnes J, Roberts AM. 2012. Comparison
1025 of conceptual landscape metrics to define hillslope-scale sediment delivery
1026 ratio. Geomorphology **138** : 74–88. DOI: 10.1016/j.geomorph.2011.08.026

1027 Vinogradova V, Gracheva R, Belonovskaya E. 2018. Climate Change Effects
1028 on Mountain Regions Marginalized by Socio-Economic Transformation—The
1029 Case of North Caucasus. In Nature, Tourism and Ethnicity as Drivers of
1030 (De)Marginalization: Insights to Marginality from Perspective of Sustainability
1031 and Development , Pelc S and Koderman M (eds). Springer International
1032 Publishing: Cham; 79–90. [online] Available from:
1033 https://doi.org/10.1007/978-3-319-59002-8_5 (Accessed 26 June 2022)

1034 Walling DE. 1983. The sediment delivery problem. Journal of Hydrology **65** :
1035 209–237. DOI: 10.1016/0022-1694(83)90217-2

1036 Wang L, Liu H. 2006. An efficient method for identifying and filling surface
1037 depressions in digital elevation models for hydrologic analysis and modelling.
1038 International Journal of Geographical Information Science **20** : 193–213. DOI:
1039 10.1080/13658810500433453

1040 Wood SN. 2011. Fast stable restricted maximum likelihood and marginal
1041 likelihood estimation of semiparametric generalized linear models. Journal of
1042 the Royal Statistical Society: Series B (Statistical Methodology) **73** : 3–36.
1043 DOI: 10.1111/j.1467-9868.2010.00749.x

1044 Wood SN, Bravington MV, Hedley SL. 2008. Soap film smoothing. Journal of
1045 the Royal Statistical Society: Series B (Statistical Methodology) **70** : 931–955.
1046 DOI: 10.1111/j.1467-9868.2008.00665.x

1047 Young A. 1960. Soil Movement by Denudational Processes on Slopes. Nature
1048 **188** : 120–122. DOI: 10.1038/188120b0

1049 Zweifel L, Meusburger K, Alewell C. 2019. Spatio-temporal pattern of soil
1050 degradation in a Swiss Alpine grassland catchment. Remote Sensing of
1051 Environment **235** : 111441. DOI: 10.1016/j.rse.2019.111441

1052

Figures

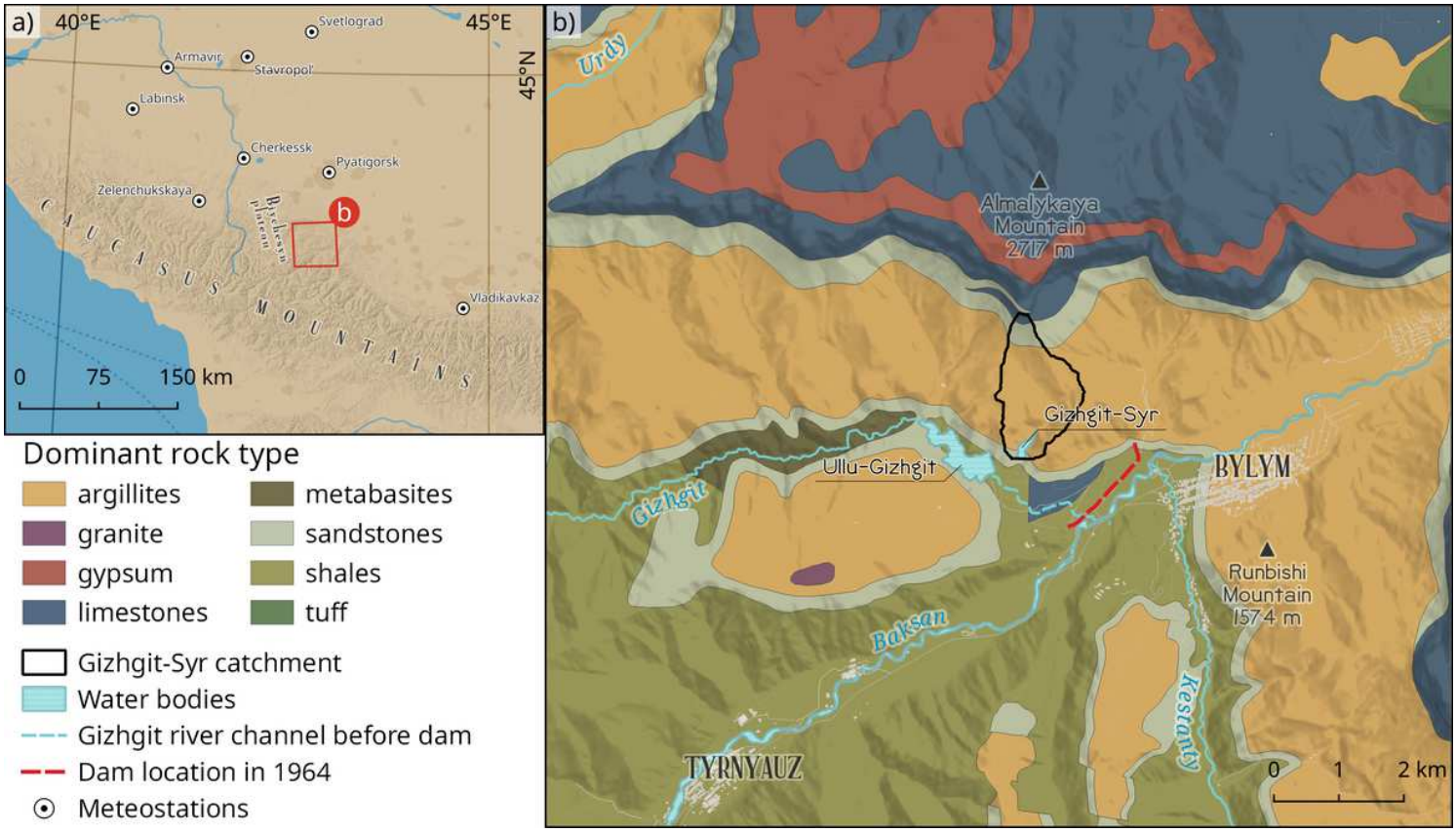

Figure 1

Map (a) shows the study area's location in the Caucasus region. Fragment of Geological map (Pismenny et al., 2021) on the study area showing the interpreted dominant rock type (b).

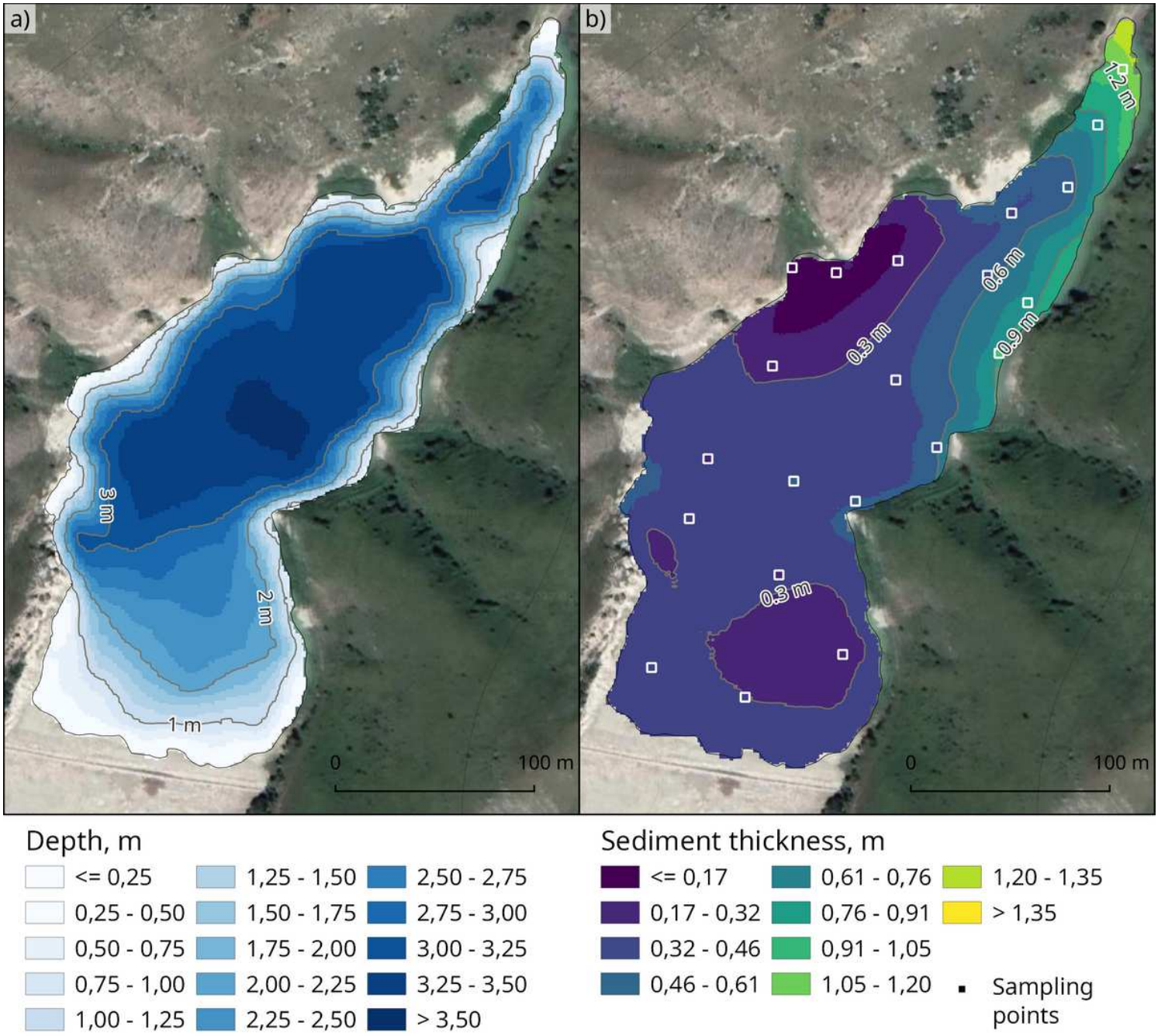

Figure 2

Lake bathymetry (a) and sediment thickness (b) map

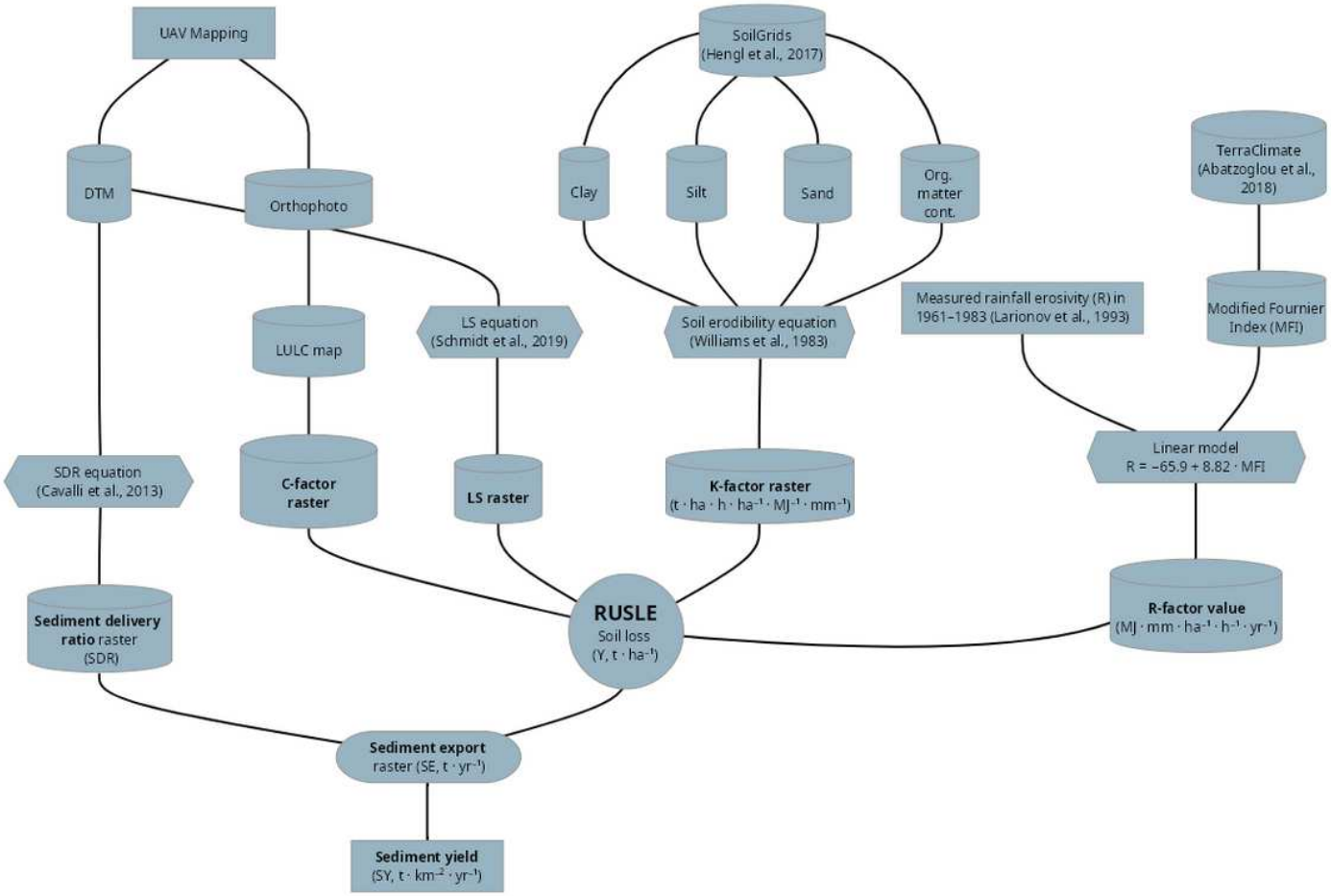

Figure 3

Here is a schematic outline of the methodological framework used to estimate the soil loss and sediment yield. Abbreviations and factors are explained in section 3.6 and supplementary material.

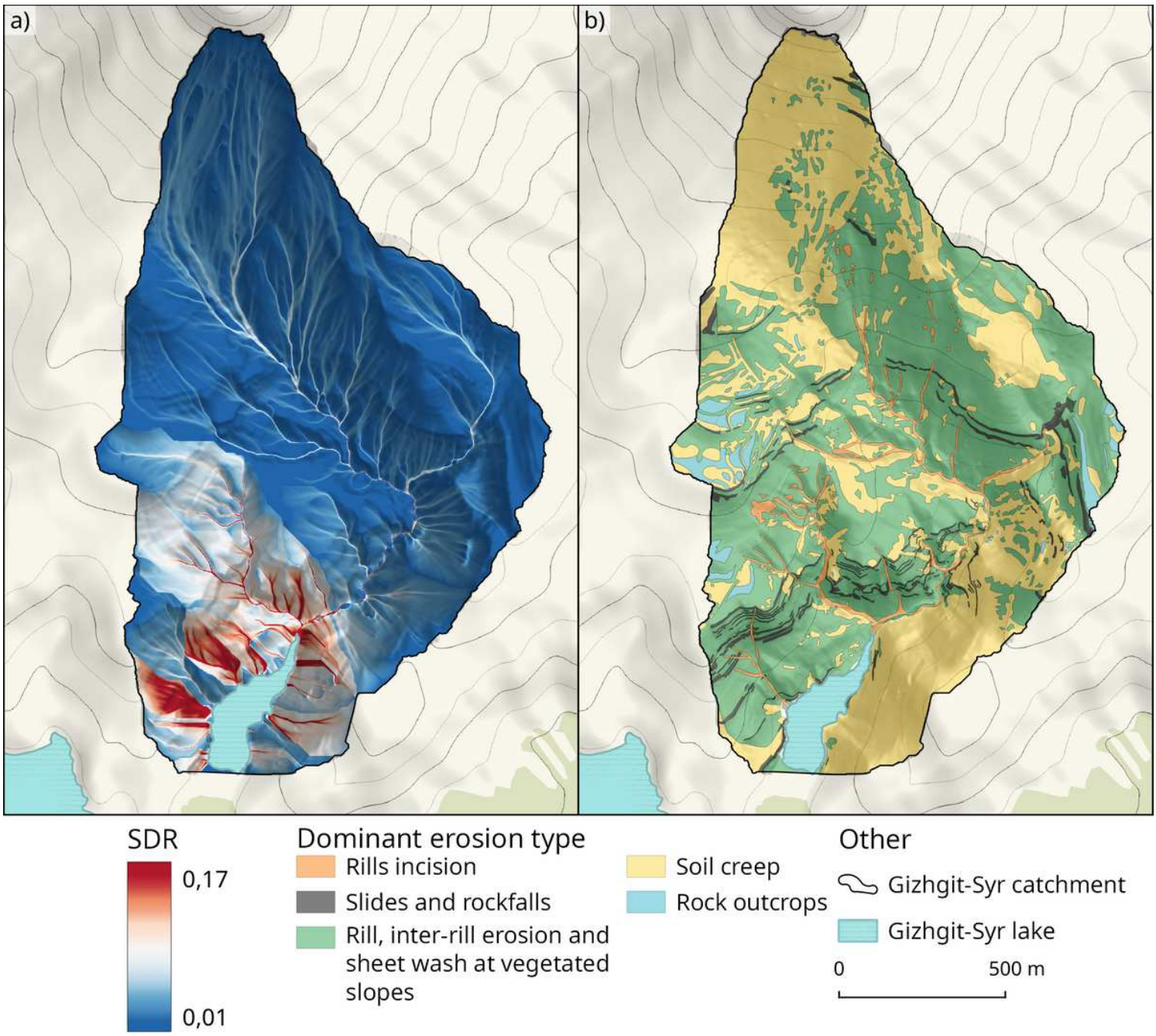

Figure 4

Sediment delivery ratio map (a) computed using Cavalli et al. (2013) approach; map of erosion types (b) digitised manually.

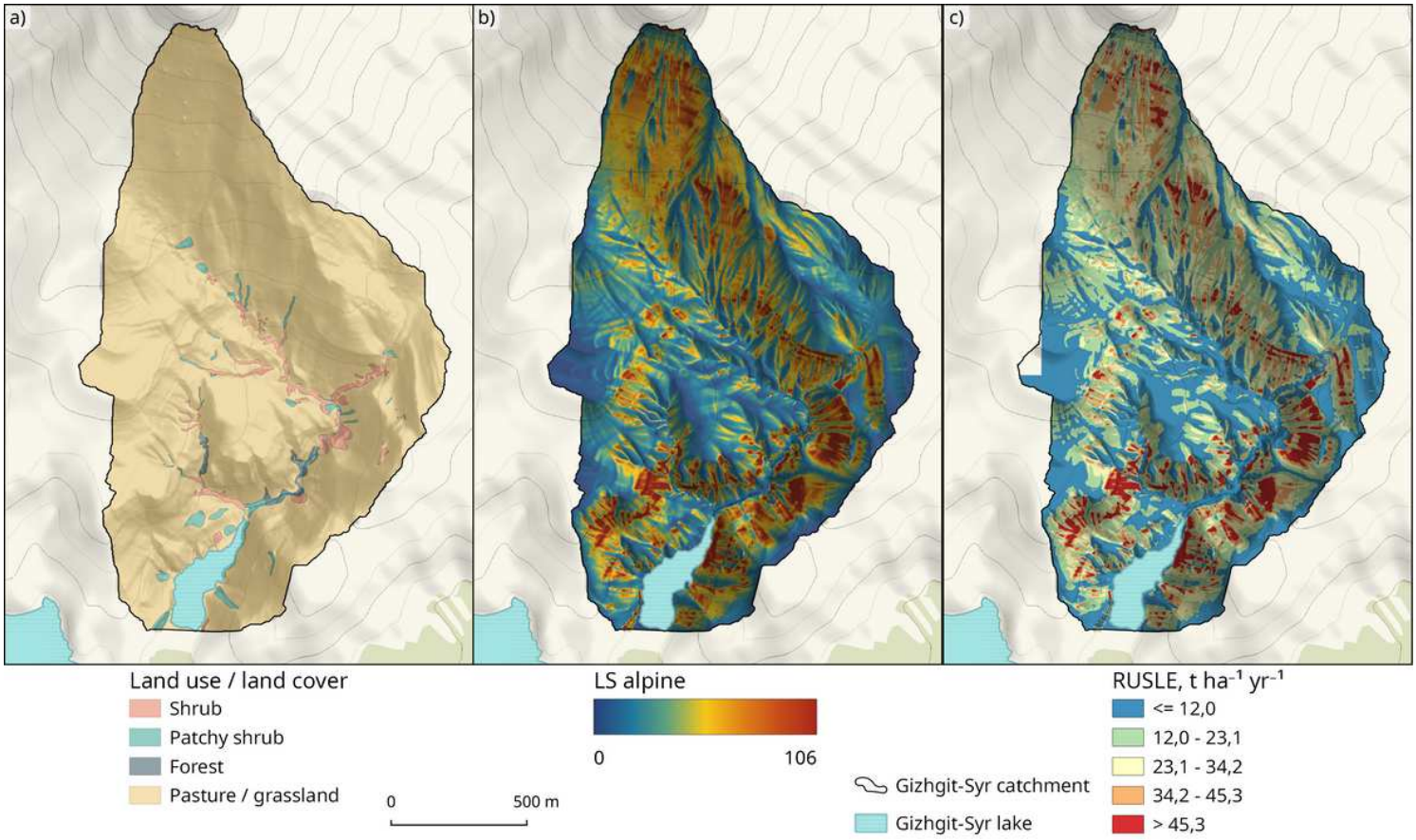

Figure 5

Land use / Land cover map of the Gizhgit-Syr catchment (a); LS_{alpine}map (b); potential soil loss due to rill and sheet erosion (RUSLE) map (c).

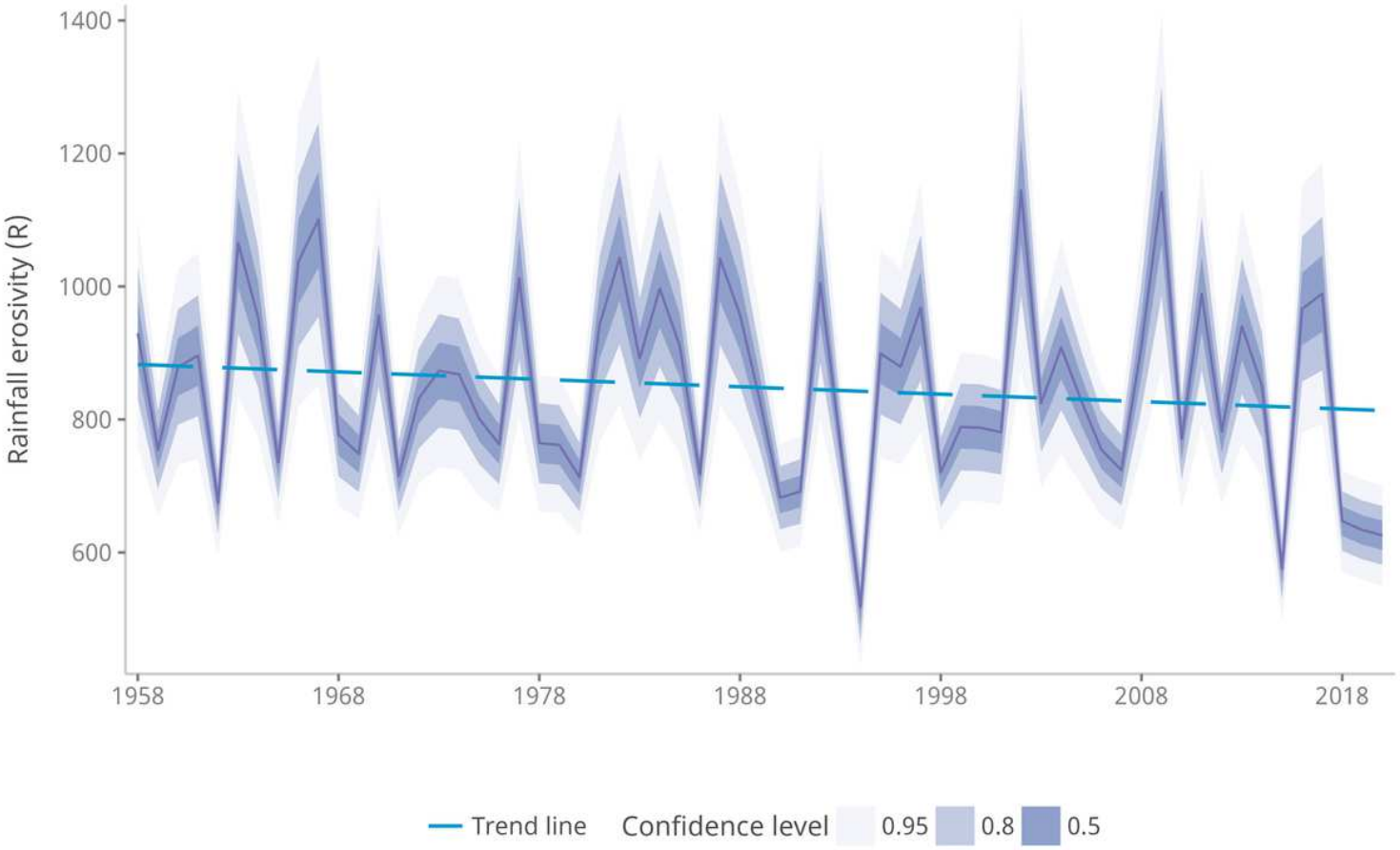

Figure 6

Rainfall erosivity time series for the Gizhgit-Syr catchment. The purple line displays the time series with the uncertainty envelope calculated with Eq. (S2). The blue line corresponds to a linear trend.

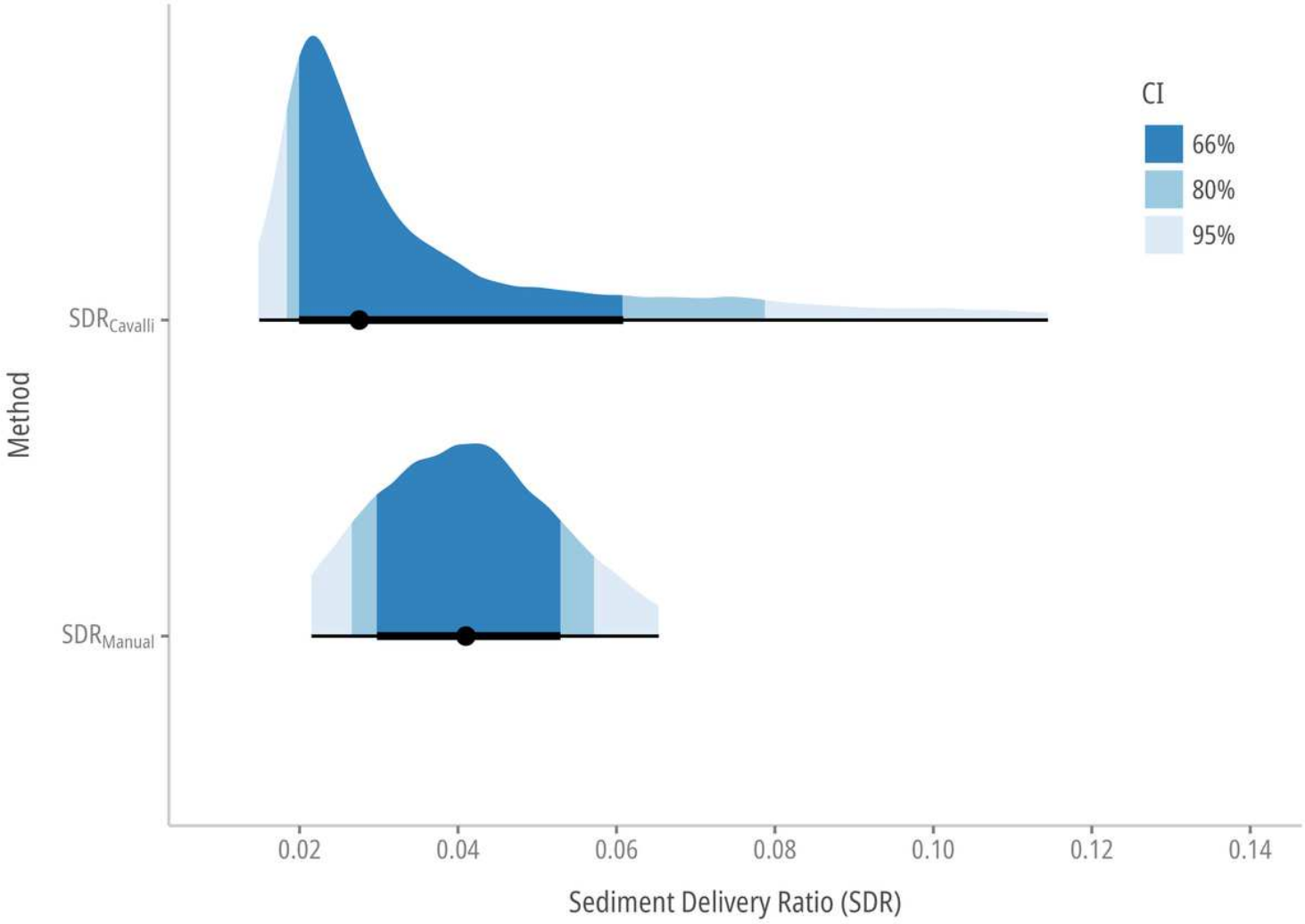

Figure 7

SDR values are computed using various methods.

Supplementary Files

This is a list of supplementary files associated with this preprint. Click to download.

- gizhgitesplSIoct2022.docx